JACS
JOURNAL OF THE AMERICAN CHEMICAL SOCIETY

Article

Sorptive Reconstruction of the CuAlCl Framework upon Reversible Ethylene Binding

Roger M. Sullivan, Haiming Liu, D. Steve Smith, Jonathan C. Hanson, Derek Osterhout, Michael Ciraolo, Clare P. Grey, and James D. Martin

J. Am. Chem. Soc., **2003**, 125 (36), 11065-11079• DOI: 10.1021/ja036172o • Publication Date (Web): 14 August 2003

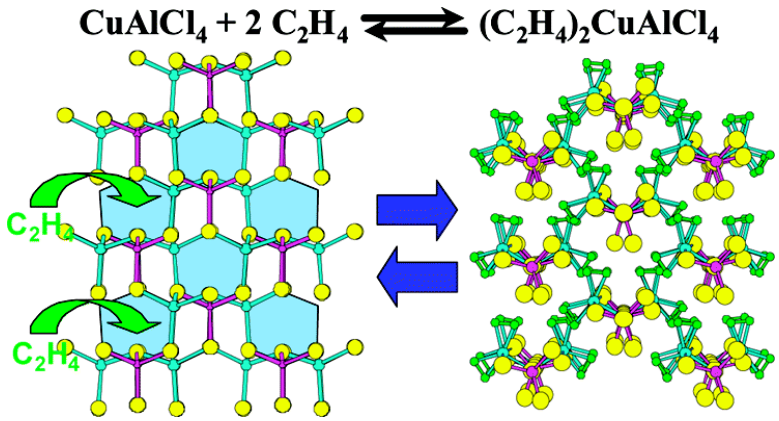

More About This Article

Additional resources and features associated with this article are available within the HTML version:

- Supporting Information
- Links to the 8 articles that cite this article, as of the time of this article download
- Access to high resolution figures
- Links to articles and content related to this article
- Copyright permission to reproduce figures and/or text from this article

View the Full Text HTML

Journal of the American Chemical Society is published by the American Chemical Society. 1155 Sixteenth Street N.W., Washington, DC 20036

J|A|C|S
ARTICLES
Published on Web 08/14/2003

Sorptive Reconstruction of the $CuAlCl_4$ Framework upon Reversible Ethylene Binding

Roger M. Sullivan,[‡] Haiming Liu,[†] D. Steve Smith,[‡] Jonathan C. Hanson,[§] Derek Osterhout,[‡] Michael Ciraolo,[†] Clare P. Grey,[†] and James D. Martin*[,‡]

Contribution from the Department of Chemistry, North Carolina State University, Raleigh, North Carolina 27695-8204, Department of Chemistry, State University of New York at Stony Brook, Stony Brook, New York 11794-3400, and Department of Chemistry, Brookhaven National Laboratory, Upton, New York 11973

Received May 15, 2003; E-mail: jdmartin@ncsu.edu

Abstract: Three ethylene adducts to $CuAlCl_4$ have been characterized by single crystal and/or powder X-ray diffraction, ^{13}C, ^{27}Al and ^{63}Cu MAS NMR and diffuse reflectance UV−vis spectroscopy. $(C_2H_4)_2CuAlCl_4$, $a = 7.1274(5)$ $b = 12.509(1)$ $c = 11.997(3)$ $\beta = 91.19°$, Pc, $Z = 4$; α-$(C_2H_4)CuAlCl_4$, $a = 7.041(3)$ $b = 10.754(8)$ $c = 11.742(9)$ $\beta = 102.48(6)$, $P2_1$, $Z = 4$ and β-$(C_2H_4)CuAlCl_4$, $a = 7.306(2)$, $b = 16.133(3)$, $c = 7.094(1)$, $Pna2_1$, $Z = 4$. Up to 2 equiv of ethylene (~200 cm^3/g relative to stp) are sorbed at room temperatures and pressures as low as 300 Torr. The ethylene ligands are bound to copper (I) primarily through a σ-interaction, because the $AlCl_4^-$ groups also bound to copper prevent any significant π-back-bonding. The olefin binding is reversible and has been characterized by gravimetric and volumetric adsorption analysis and by time and pressure resolved synchrotron powder X-ray diffraction. Comparison of the parent crystal structure to those of the adduct phases provide an atomistic picture of the sorptive reconstruction reactions. These are proposed to proceed by a classic substitution mechanism that is directed by the van der Waals channels of the parent crystalline lattice.

Introduction

Copper(I) compounds exhibit considerable utility in olefin production and processing for both separations and catalysis. In particular, their use in facilitated transport membranes is under active investigation to develop replacements for energetically costly cryogenic separations of olefins from paraffins.[1−5] Nature, like industry, has recognized the beneficial role of Cu(I) in the reversible binding of olefins. For example, Cu(I) is implicated as the ethylene receptor in metalloenzymes, where ethylene serves as a growth hormone.[6] With respect to catalysis, late transition metal copper(I) complexes have recently been demonstrated to be attractive candidates for polymerization of olefins with polar functional groups,[7] and copper (I) plays a crucial role in the oxychlorination of ethylene.[8] Despite the economic importance of simple cuprous salts in binding olefins, relatively little structural and mechanistic information is available due in part to the inherent instability of these materials with respect to loss of ethylene.[9] Furthermore, there is a paucity of mechanistic information probing the reaction of small molecules with bulk crystalline solids that are neither surface reactions nor reactions within a porous host.[10,11] Nevertheless, some condensed crystalline solids are well-known to sorb small molecules, for example H_2 and H_2O, and maintain crystallinity throughout substrate binding and release, although more is understood about the mechanisms of desorption/decomposition than the mechanisms of sorption.[12] In this work, we describe the reversible binding of ethylene to $CuAlCl_4$ providing the first crystal structures of ethylene bound to simple metal-halide salts

[†] State University of New York at Stony Brook.
[‡] North Carolina State University.
[§] Brookhaven National Laboratory.

(1) Gilliland, E. R. Recovery of Olefins. U.S. Patent, 2,289,773, 1942.
(2) *Separation Technologies for the Industries of the Future*; National Research Council (US), National Academy Press: Washington, DC, 1998.
(3) Kim, Y. H.; Ryu, J. H.; Bae, J. Y.; Kang, Y. S.; Kim, H. S. *Chem. Commun.* **2000**, 195−196.
(4) Kim, H. S.; Kim, Y. J.; Kim, J. J.; Lee, S. D.; Kang, Y. S.; Chin, C. S. *Chem. Mater*. **2001**, *13*, 1720−1725.
(5) Takahashi, A.; Yang, R. T.; Munson, C. L.; Chinn, D. *Langmuir* **2001**, *17*, 8405−8413.
(6) Rodríguez, F. I.; Esch, J. J.; Hall, A. E.; Binder, B. M.; Schaller, G. E.; Bleeker, A. B. *Science* **1999**, *283*, 996−998.
(7) Stibrany, R. T.; Shultz, D. N.; Kacker, S.; Patil, A. O. U.S. Patent 6,037,297, Mar. 14, 2000.
(8) Neurock, M.; Zhang, X.; Olken, M.; Jones, M.; Hickman, D.; Calverley, T.; Gulotty, R. *J. Phys. Chem. B* **2001**, *105*, 1562−1573.
(9) (a) Thompson, J. S.; Harlow, R. L.; Whitney, J. F. *J. Am. Chem. Soc.* **1983**, *105*, 3522−3527. (b)Thompson, J. S.; Whitney, J. F. *Inorg. Chem.* **1984**, *23*, 2813−2819. (c) Masuda, H.; Yamamoto, N.; Taga, T.; Machida, K.; Kitagawa, S.; Munakata, M. *J. Organomet. Chem.* **1987**, *322*, 121−129. (d) Munakata, M.; Kuroda-Sowa, T.; Maekawa, M.; Nakamura, M.; Akiyama, S.; Kitagawa, S. *Inorg. Chem.* **1994**, *33*, 1284−1291. (e) Suenaga, Y.; Wu, L. P.; Kuroda-Sowa, T.; Munakata, M.; Maekawa, M. *Polyhedron* **1997**, *16*, 67−70. (f) Dai, J.; Yamamoto, M.; Kuroda-Sowa, T.; Maekawa, M.; Suenaga, Y.; Munakata, M. *Inorg. Chem.* **1997**, *36*, 2688−2690. (g) Straub, B. F.; Eisentrager, F.; Hofmann, P. *Chem. Commun.* **1999**, 2507−2508 (h) Dai, X.; Warren, T. H. *Chem. Commun*. **2001**, 1998−1999. (i) Dias, H. V. R.; Lu, H.-L.; Kim, H.-J.; Polach, S. A.; Goh, T. K. H. H.; Browning, R. G.; Lovely, C. J. *Orgonometallics* **2002**, *21*, 1466−1473.
(10) Albrecht, M.; Lutz, M.; Spek, A. L.; van Koten, G. *Nature* **2000**, *406*, 970−974.
(11) Kitaura, R.; Seki, K.; Akiyama, G.; Kitagawa, S. *Angew. Chem., Int. Ed. Engl*. **2003**, *42*, 428−431.
(12) (a) *Reactions of Solids with Gases, Comprehensive Chemical Kinetics, Vol 21*; Bamford, C. H., Tipper, C. F. H., Compton, R. G., Eds.; Elsevier: Amsterdam, 1984. (b) *Reactions in the Solid State, Comprehensive Chemical Kinetics*; Bamford, C. H., Tipper, C. F. H., Eds.; Elsevier: Amsterdam, 1980; Vol 22.

and the first crystal structure of a bis-ethylene adduct to Cu(I). From an understanding of these crystalline structures along with time and pressure resolved diffraction and spectroscopic studies, we propose an atomistic description of the mechanism by which the $CuAlCl_4$ crystalline lattice is transformed during the reversible sorption of ethylene.

Background

Part of copper's attraction to both industry and living organisms is undoubtedly its ready availability and relatively low toxicity. In addition, the electronic structure of copper(I) imparts a distinctive reactivity particularly well suited for the reversible binding of olefins.[13,14] With its d^{10}-electronic configuration, the highest lying filled orbitals exhibit a M−L σ^* character, however, these can also serve as π-backing bonding orbitals to other ligands when the metal exhibits tetrahedral or trigonal planar coordination. Because copper's electronegativity is similar to that of silicon, there is a significant covalency in the Cu−L bonds even when L is chlorine. The electronegativity of Cu (I) also results in the relatively low-lying and empty 4s and 4p orbitals, which are well poised to act as an acceptor of σ-electron density. The relative energy of the π- and σ-type metal-based orbitals significantly influence the ability of a metal to bind olefins. For example, among isoelectronic metal complexes, no crystal structures with ethylene bound to Zn(II) are reported in the Cambridge Structural Database, whereas 13 structures are reported with Cu(I),[9] and 29 structures of Ni(0)-ethylene complexes, which exhibit a greater propensity for metal-ethylene back-bonding, are reported. The choice of ancillary ligands bound to the metal center further tune the energy of these metal-based orbitals. The π-back-bonding ability of the metal can be increased with strongly Lewis-basic ligands such as amines and phosphines, as is observed for all of the previously reported Cu(I)-ethylene crystal structures.[9] In contrast, although electron withdrawing (Lewis acidic) ligand environments will decrease the π-back-bonding ability, these will also lower the energy of the empty Cu 4s and 4p orbitals which can result in stronger metal-olefin σ-interactions. A similar range of bonding interactions was recently reported for Cu(I)-carbonyl complexes where Cu−CO back-bonding was favored with strong donor ancillary ligands, but nonclassical carbonyl complexes (resulting from strong σ interactions with little to no π-back-bonding) are formed with more Lewis acidic ancillary ligands.[15] Nature in metalloenzymes, and numerous bioinorganic model complexes, has controlled the Cu(I)-olefin binding by manipulating the π-back-bonding with strong donor ancillary ligands. Much less attention has been paid to the reactivity of Cu(I) in a Lewis acidic environment, such as CuCl with $AlCl_3$, although this too should enhance metal-olefin binding.[16,17]

The reactivity of CuCl with olefins in both solution and the solid state is well-known, although structurally the complex product(s) is rather poorly characterized because high pressure and low temperature are required for complex formation.[8,18−20] The affinity of CuCl for olefins is greatly enhanced when in the presence of a very strong Lewis acid such as $AlCl_3$. Toluene solutions of, and polymers impregnated with, $CuAlCl_4$ are reported for the separation of olefins and CO from various feed streams.[21] The $CuCl/AlCl_3$ system is used as a homogeneous catalyst for the preparation of polyphenylene conductive polymers,[22] extended all benzenoid hydrocarbons,[23] the formylation of aromatic compounds,[24] the synthesis of carbonic acid dialkyl, alkyl, aryl or cycloalkyl esters from CO and alcohols,[25] and as a cocatalyst with $Al(C_2H_5)_nCl_{3-n}$ for the oligomerization of olefins.[26] Nevertheless, prior to this work, the crystal structure of η^2-$(C_6H_6)CuAlCl_4$ was the only structurally characterized adduct phase,[27] and the benzene is readily lost from the adduct to reform α-$CuAlCl_4$.[28] All prior crystal structures of ethylene adducts to Cu(I) are found in the bioinorganic literature.[9] None of these works begin to address the mechanism by which small molecules such as olefins and aromatics can be transported through a bulk crystalline lattice.

The crystalline structures and spectroscopic characterization of novel ethylene adducts to α- and β-$CuAlCl_4$, and $CuGaCl_4$ (and lack of reactivity with $CuAlBr_4$) are reported here. Three different $CuAlCl_4$ ethylene adducts were first identified in volumetric adsorption, gravimetric and time/pressure resolved synchrotron diffraction studies. Structures of two of the adducts are solved by single-crystal X-ray diffraction methods, whereas a model for the third structure, based on powder diffraction studies and NMR is presented. These results provide mechanistic insight into the deconstruction and reconstruction of the metal halide lattice upon ethylene sorption/desorbtion. The atomistic picture of the sorptive reconstruction developed in this study suggests that small changes in the reaction conditions can determine whether the reactions proceed via a diffusion-controlled or a phase boundary-controlled reaction mechanism.

Results

Adsorption Isotherm Measurements. To elucidate the uptake of ethylene adducts by copper aluminum chloride, volumetric adsorption and gravimetric measurements were conducted. When exposed to an ethylenepressure of 1800 Torr at room temperature α-$CuAlCl_4$ exhibited an uptake of 2 mol equiv of ethylene. Similar gravimetric experiments showed no significant uptake of ethylene at 1800 Torr by the isostructural α-$CuAlBr_4$. The reaction of ethylene with $CuAlCl_4$ is exothermic. When a sample, fully loaded with 2 equiv of ethylene and maintained under a constant pressure of 1800 Torr, is heated in the gravimetric apparatus the solid begins to melt at 42 °C. At around 65 °C, a noticeable effervescence accompanies the melting process. The evolution of gas is observed to cease at

(13) (a) Dewar, M. *Bull. Soc. Chim. Fr.* **1951**, *18*, C79. (b) Chatt, J.; Duncanson, L. *J. Chem. Soc.* **1953**, 2939−2947.
(14) Albright, T. A.; Hoffmann, R.; Thibeault, J. C.; Thorn, D. L. *J. Am. Chem. Soc.*, **1979**, *101*, 3801−3812.
(15) Strauss, S. H. *J. Chem. Soc., Dalton Trans.* **2000**, 1−6.
(16) Dattelbaum, A. M.; Martin, J. D. *Inorg. Chem.* **1999**, *38*, 6200−6205.
(17) Suzuki, T.; Nobel, R. D.; Koval, C. A. *Inorg. Chem.* **1997**, *36*, 136−140.
(18) Berthelot, *Ann. Chem. Phys.* **1901**, *23*, 32−39.
(19) Tropsch, H.; Mattox, W. J. *J. Am. Chem. Soc.* **1935**, *57*, 1102−1103.
(20) Gilliland, E. R.; Seebold, J. E.; FitzHugh, J. R.; Morgan, P. S. *J. Am. Chem. Soc.* **1939**, *61*, 1960−1962.
(21) Long, R. B.; Caruso, F. A.; Walker, D. G. Monomere Bimetellsalze sowei Verfahren zu ihrer Herstellung and Verbindung. German Patent, DE 1,-944,405, 1968. (b) Sudduth, J. R.; Keyworth, D. A. Process for the Purification of Gas Streams. U.S. Patent 3,960,910, 1975.
(22) Hirai, H.; Wada, K.; Komiyama, M. *Bull. Chem. Soc. Jpn.* **1986**, *59*, 1043−1049.
(23) Müller, M.; Kubel, C.; Müllen, K. *Chem. Eur. J.* **1998**, *4*, 2099−2109.
(24) Gatterman, L.; Koch, H. *Chem. Ber.* **1897**, *30*, 1622−1624.
(25) Gänzler, W.; Schröder, G. Verfahren zur Herstellung von Kohlensäureestern. German Patent DE 2,520,708, Nov. 25, 1976.
(26) Johnson, B. H. Catalysis for the polymerization of olefins to yield predominantly dimers and trimers. U.S. Patent 3,475,347, Oct. 28, 1969.
(27) Turner, T. W.; Amma, E. L. *J. Am. Chem. Soc.* **1966**, *88*, 1877−1882.
(28) Martin, J. D.; Leafblad, B. R.; Sullivan, R. M.; Boyle, P. D. *Inorg. Chem.* **1998**, *37*, 1341−1346.

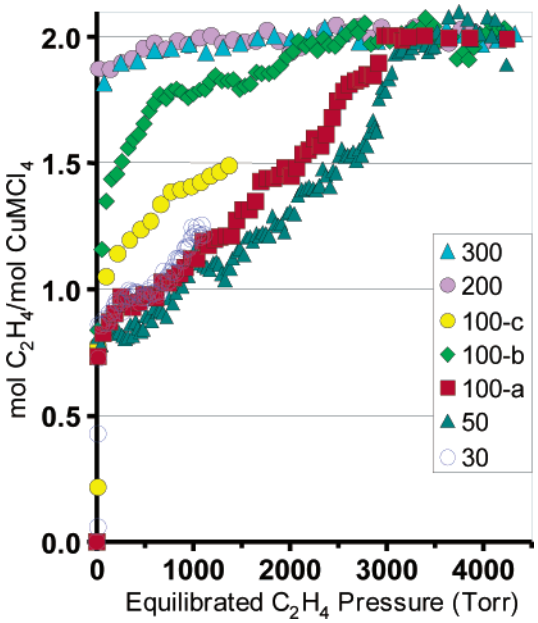

Figure 1. The volumetric adsorption of ethylene by α-$CuAlCl_4$. The pressure step size for each room-temperature isotherm is indicated in the figure legend.

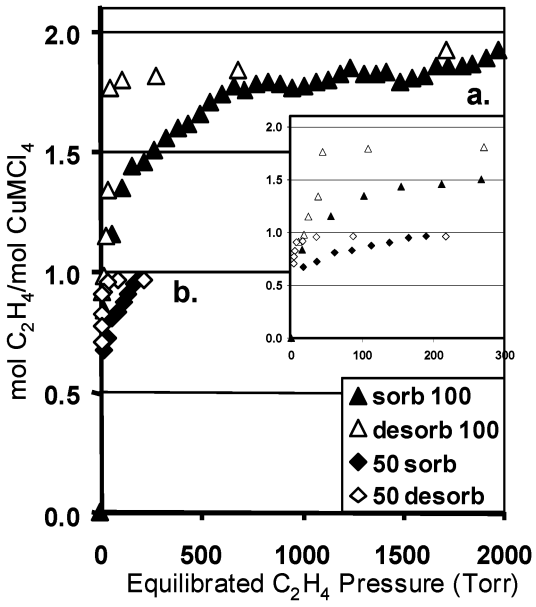

Figure 2. Volumetric adsorption/desorption isotherms for (a) 100 Torr step size sorption to **et-2** followed by desorption, and (b) 50 Torr step size sorption to **et-1** followed by desorption. The inset, plotted at an expanded scale, highlights the difference between the equilibrium binding pressure for the two- and one-equivalent adducts.

87 °C. By gravimetric determination, the melt is observed to retain one equivalent of ethylene. Further heating to approximately 200 °C appears to drive off all of the ethylene.

Representative examples of the volumetric adsorption/desorption experiments run under a variety of reaction conditions are presented in Figure 1, plotted as the number of moles of ethylene sorbed per mole of $CuAlCl_4$ vs the equilibrated pressure of ethylene. Although data from identical experiments are equivalent, variations in the conditions of the sorption experiment exhibit significant sample history dependence. Samples were exposed to various initial ethylene pressures and to subsequent doses with varying size steps in the ethylene pressure (see the Experimental Section). In the sorption run 100-a, an inflection in the sorption curve at approximately 1 equiv of ethylene is observed at around one atmosphere of ethylene pressure. A second equiv of ethylene is gradually sorbed with increasing pressure up to the maximum sorption of 2 molar equiv of ethylene by about 3000 Torr. Similar results are obtained for the sorption isotherms measured with 30 and 50 Torr steps of ethylene pressure. By contrast, sorption experiments performed with an initial ethylene exposure pressure of greater than 100 Torr (runs 200 and 300 in Figure 1) demonstrate an immediate sorption of two equivalents of ethylene. No further ethylene was sorbed up to the 5000 Torr limiting pressure of our line. The greatest variability in volumetric adsorption measurements was observed for runs with an initial line pressure and step size of 100 Torr. Variability between runs could approximately be correlated with the freshness of the sample, and prebaking the gas line (100 °C under vacuum) and possibly the temperature. The data plotted as 100-a represent the low sorption extreme normally observed with fresh samples of $CuAlCl_4$ and after baking the line. The data plotted as 100-b in Figure 1 represent the high sorption extreme observed for samples that had been stored in the glovebox for more than a month. The runs were also performed at slightly different temperatures (297, 294, and 296 K for runs 100-a, b, and c, respectively), which may account for some of the variability. These 100 Torr-step runs differ primarily in the amount of initial ethylene sorbed, but exhibit a similar slope for the higher-pressure sorption.

A significant hysteresis is observed between the sorption and desorption of ethylene from $CuAlCl_4$, Figure 2. In the experiment of Figure 2a, a sample was exposed to conditions similar to that of run 100-b to form the two-equivalent adduct. No desorption was observed until the pressure was reduced to below 100 Torr. In the experiment of Figure 2b, the sample was exposed to reaction conditions similar to the isotherm 50 of Figure 1. However, this sorption run was stopped at the equilibrated pressure of 217 Torr consistent with near complete formation of a one-equivalent adduct. The sample was then stepwise evacuated, and no desorption was observed until pressures below 20 Torr. Complete desorption was not achieved in these room temperature isotherms, though heating the sample was observed to force greater ethylene desorption. Powder diffraction measurements of a desorbed sample showed only the presence of the α-$CuAlCl_4$.

The data from volumetric adsorption isotherms with $CuGaCl_4$ demonstrate a diminished binding efficiency for the material with gallium compared to aluminum (Figure 1, Supporting Information). Isotherms for ethylene sorption into $CuGaCl_4$ with both 100 and 300 Torr steps in ethylene pressure show equivalent sorption characteristics, which indicate sorption of only one equivalent of ethylene by about 1500 Torr, and the gradual further sorption up to an additional half equivalent by 4000 Torr.

Variable Pressure Powder X-ray Diffraction. In situ synchrotron powder X-ray diffraction measurements, performed as a function of ethylene pressure, time, and temperature were performed to identify the different phases implicated in the volumetric adsorption measurements. A precise comparison between the adsorption isotherm and diffraction measurements

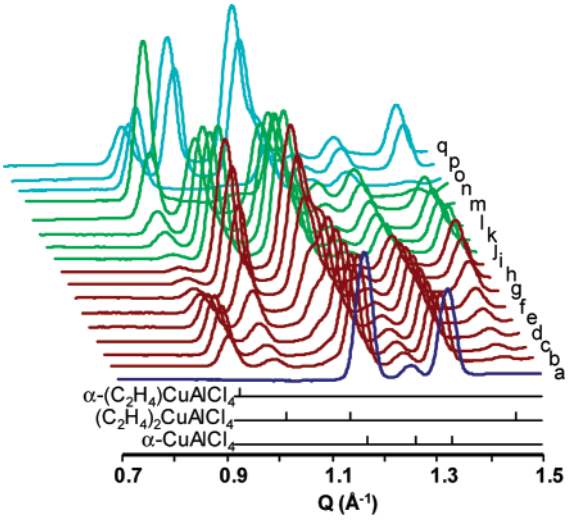

Figure 3. Pressure and time resolved synchrotron X-ray diffraction data for the sorption and desorption of ethylene into α−$CuAlCl_4$ [diffractogram: pressure of ethylene (Torr), time (h)]. Initial (dark blue line), ***a***: vac., 0. Sorption of ethylene (brown lines), ***b***: 100, 0.3; ***c***: 200, 3.5; ***d***: 300, 3.8; ***e***: 400, 4.1; ***f***: 500, 4.7; ***g***: 800, 5.8; ***h***: 1200, 7.5; ***i***: 1600, 10.5. Desorption of ethylene (green lines), ***j***: vac., t = 0; ***k***: 0.030, 1.0; **l**: 0.025, 2.0; ***m***: 0.025, 3.0; ***n***: 0.023, 4.0. Re-sorption of ethylene (light blue lines), ***o***: 0.02, 0; ***p***: 1400, 0.3; ***q***: 1400, 1.0. These data were obtained with the sample cooled to 15 °C and then warmed to room temperature for the last desorption diffractogram, ***n***, and the resorption experiment, ***o***−***q***. Histograms at the base of the figure indicate the characteristic diffraction peaks of α-$CuAlCl_4$, **α-et-1** and **et-2**.

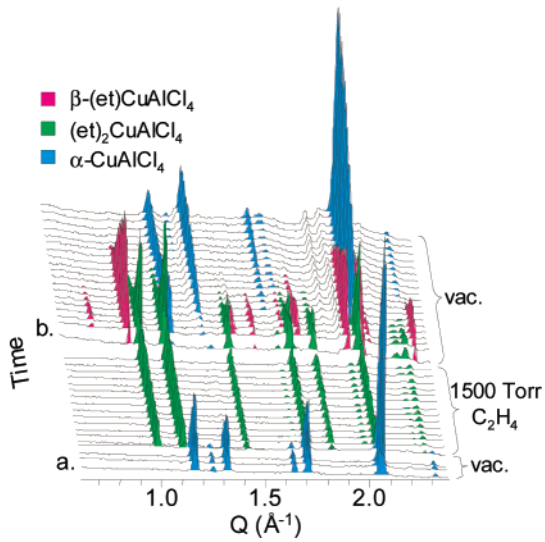

Figure 4. Time-resolved variable atmosphere powder X-ray diffractograms for the formation of (a) **et-2** by exposure of α-$CuAlCl_4$ to 1500 Torr of ethylene, and (b) ***β*-et-1** and α-$CuAlCl_4$ upon desorption.

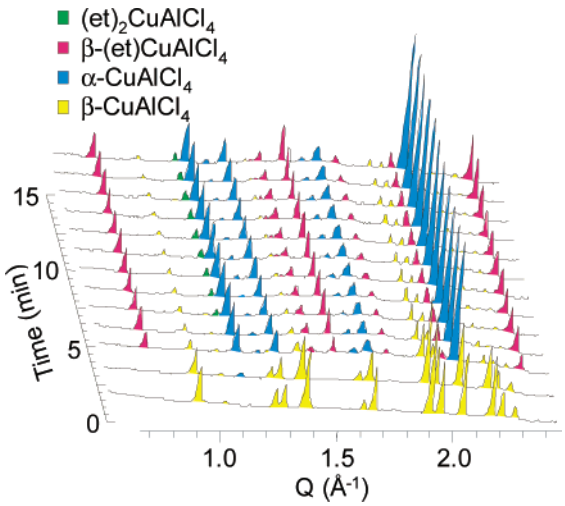

Figure 5. Time resolved, variable atmosphere, powder X-ray diffractograms showing the conversion of *β*-$CuAlCl_4$ to ***β*-et-1** and α-$CuAlCl_4$ upon exposure to 100 Torr of ethylene.

Table 1. Characteristic, Low Angle Reflections for Identifying Phases in Powder X-ray Diffractograms

phase	hkl	Q (Å^{-1})
α-$CuAlCl_4$	100	1.15
	002	1.24
	101	1.31
β-$CuAlCl_4$	110	0.96
	210	1.28
	011	1.31
	111	1.40
$(C_2H_4)_2CuAlCl_4$	110	1.00
	021/11−1	1.12
α-$(C_2H_4)CuAlCl_4$	001	.55
	100	0.92
β-$(C_2H_4)CuAlCl_4$	002	0.78
	110	0.94
	120	1.16

is complicated by the ethylene pressure gradient observed for samples loaded into capillaries for the diffraction experiments. An ethylene pressure gradient is inferred from the observation that more ethylene rich phases form at the end of the capillary open to the gas and ethylene free phases are observed at the opposite end. To control these capillary diffusion effects, all data presented here were obtained with the synchrotron X-ray beam focused on the front face of the sample, which we presume to be most analogous to the thin layer of powdered sample utilized in the volumetric adsorption experiments. Diffractograms from representative experiments of more than 50 runs, under varying experimental conditions, are presented in Figures 3−5 and Supplementary Information Figure 2. These experiments demonstrate the interrelationship between three ethylene adduct phases, α-$C_2H_4CuAlCl_4$, *β*-$C_2H_4CuAlCl_4$, and $(C_2H_4)_2$-$CuAlCl_4$, which are hereafter denoted as **α-** and ***β*-et-1**, and **et-2**, respectively. These ethylene adduct phases can readily be differentiated from each other and from the α- or *β*-$CuAlCl_4$ starting materials based on the low reciprocal space diffraction lines as summarized in Table 1.

In the diffraction experiment, shown in Figure 3, that resembles the 100 Torr step volumetric adsorption experiments of Figure 1, a sample of α-$CuAlCl_4$ cooled to 15 °C, was exposed to 100 Torr of ethylene followed by subsequent exposures to 100 Torr stepwise increases in ethylene pressure to 1600 Torr over 10.5 h. In addition, diffraction data were obtained for the partial desorption and resorption of ethylene from this sample. In Figure 3, diffractogram b, taken after 20 min of equilibration at 100 Torr, a mixture of **α-et-1**, the α-$CuAlCl_4$ starting material, as well as a small amount of the two-equivalent adduct, **et-2**, is observed. The pressure was increased to 200 Torr and equilibrated for an additional 3.2 h prior to diffractogram Figure 3c, in which the amount of **α-et-1** is observed to increase, but there is little to no change in the amount of **et-2**. Above 300 Torr of ethylene pressure (Figure 3d-i) the diffractograms demonstrate an increase in the amount of the **et-2** at the expense of the **α-et-1**. At an ethylene pressure of 1600 Torr, the conversion

of the **α-et-1** to **et-2** is nearing completion. Some of the parent α-$CuAlCl_4$ starting material persists throughout this reaction, though it continually diminishes in intensity. The persistence of α-$CuAlCl_4$ is attributed to incomplete diffusion of the ethylene through the sample in the capillary. Evacuation of this sample (Figure 3j−n) results in the return of the **α-et-1** phase now at the expense of the **et-2** phase. Under these in situ conditions, at 15 °C, full desorption from the one-equivalent adduct back to the parent starting material was not observed. A significant increase in desorption was observed after warming the sample to room temperature (Figure 3o). Re-exposure to 1400 Torr of ethylene pressure at room-temperature again resulted in the conversion of the one-equivalent adduct to the two-equivalent ethylene adduct (Figure 3p−q).

In a second experiment, a fresh sample of α-$CuAlCl_4$ was exposed to an initial pressure of 1500 Torr ethylene at room temperature. After a half-hour under two atmospheres of ethylene pressure, the sample was exposed to dynamic vacuum to monitor the structural transformation upon desorption. These data, presented in Figure 4, consist of two TIP image plates, each exposed for 30 min at room temperature, such that each slice of the diffractogram shown in the figure corresponds to an average over 100 s. Careful examination of the fourth diffractogram of Figure 4a (the first diffractogram after the sample was exposed to ethylene) demonstrates that both the parent α-$CuAlCl_4$, and the **et-2** adduct phase are present simultaneously without any evidence for a one-equivalent intermediate phase. By the fifth diffractogram, the reaction is complete with only the two-equivalent adduct being observed. Immediately upon exposure to vacuum the diffraction intensity of the two-equivalent adduct phase begins to decrease with the growth of a new one-equivalent intermediate phase, Figure 4b. The diffraction fingerprint of this one-equivalent adduct is distinct from that of **α-et-1** observed in Figure 3, but is equivalent to that calculated from the single-crystal determination of ***β*-et-1** (see below). This one-equivalent intermediate is observed to grow in intensity for the first 8−10 min of evacuation, and then it too is lost to the reformation of the parent $CuAlCl_4$ material. There remain a few as yet unaccounted for reflections in the evacuated diffractogram. Possible assignments include β-$CuAlCl_4$ or a proposed γ-$CuAlCl_4$ polymorph based on the orthorhombic $CuGaI_4$ structure-type.[29] Whatever the actual structure of these unidentified phase(s), they appear to be metastable with respect to α-$CuAlCl_4$ because all samples that have been ground and reloaded into capillaries after sorption and desorption exhibit exclusively α-$CuAlCl_4$.

To trap a one-equivalent intermediate from a higher pressure reaction, or to confirm that the higher pressure reactions proceed by a direct conversion of α-$CuAlCl_4$ to the two-equivalent adduct, an evacuated capillary loaded with α-$CuAlCl_4$ was cooled to 100 K and then exposed to 1500 Torr of ethylene pressure. These data, shown in supplemental information Figure 2, demonstrate that after one minute of exposure to ethylene, a small amount of **et-2** is formed. But there is no evidence for the formation of either one-equivalent-adduct phase. Under these low-temperature conditions, however, this reaction is not observed to proceed beyond about 10%.

When a sample of β-$CuAlCl_4$ was exposed to 100 Torr of ethylene pressure, a slightly different reaction pathway was observed, indicated by the data presented in Figure 5. In the second diffractogram, immediately after exposure to ethylene, the onset of a conversion from the metastable β-$CuAlCl_4$ polymorph to the thermodynamically stable α-$CuAlCl_4$ is observed.[30] In addition to the continued β → α-$CuAlCl_4$ transformation, the onset of the formation of ***β*-et-1** is observed in the third diffractogram. By the fourth diffractogram, the first sign of the formation of the two-equivalent adduct **et-2** is observed, although because of crystallite preferred orientation its identification is only confirmed by a full-plate exposure taken at the end of this experiment after raising the ethylene pressure to 1000 Torr.

The specific reaction conditions leading to the respective formation of the α- and β-ethylene adducts remains unresolved. To date, low-pressure reactions with β-$CuAlCl_4$ have only yielded ***β*-et-1**. Low-pressure reactions with α-$CuAlCl_4$ normally yield **α-et-1**, however, reactions in which some atmospheric moisture may have entered the capillary while loading onto the gas-line goniometer head also yielded ***β*-et-1**. The intermediate ***β*-et-1** has also been observed upon desorption from the two-equivalent adduct, or as the one-equivalent phase that is grown out of a melt under an ethylene atmosphere.

α-$CuGaCl_4$ is also observed to undergo a major reconstruction upon sorption of ethylene. Upon exposure of a sample of α-$CuGaCl_4$ to an ethylene pressure of 1500 Torr a diffraction pattern that is similar to that of **α-et-1** is observed. Its diffraction pattern can be indexed to the monoclinic cell $a = 7.017(3)$, $b = 10.765(4)$, $c = 11.768(8)$, and $\beta = 103.31(3)$ (Supporting Information Figure 4). The formation of a one-equivalent ethylene adduct to $CuGaCl_4$ at this pressure is consistent with the adsorption experiments reported above. Ethylene pressures sufficient to provide evidence of a two-equivalent adduct have not yet been achieved with our diffraction gas line.

X-ray Crystal Structures. Single crystals were grown for **et-2**, and ***β*-et-1**, and their crystal structures were determined by X-ray diffraction. X-ray powder patterns calculated from the structures confirmed the assignments of the single crystals to the specific phases identified in the in situ powder diffraction experiments. Unfortunately, we have not yet been able to grow a single crystal of **α-et-1**, but a model for the structure of **α-et-1** is proposed based on a partial structural solution of this phase, by powder methods. A summary of the crystallographic data for these is given in Table 2. Full details of the structure solutions are available in supplementary information.

$(C_2H_4)_2CuAlCl_4$, et-2. The structure of **et-2** can be described as a $(C_2H_4)_2CuAlCl_4$ molecular-type unit with strong intermolecular interactions forming 1-D chainlike structures that run parallel to the **c**-axis, as shown in Figure 6. In the low-temperature crystal structure the monoclinic space group, Pc, yields two crystallographicly independent chains that show only trivial deviations in bond lengths and angles. Upon warming to room temperature the structure exhibits a 4.2% expansion in unit cell volume with apparent transformation to an orthorhombic lattice and the space group $P2_1cn$, a supergroup of *Pc*, as determined by a Rietveld refinement using synchrotron powder X-ray diffraction data. In the orthorhombic space group, the two chains are rendered equivalent by the 2_1 and *n*-glide symmetry operations.

(29) Burns, R.; Zajonc, A.; Meyer, G. *Z. Kristalloger.* **1995**, *210*, 62.

(30) Liu H.; Sullivan, R. M.; Hanson, J. C.; Grey, C. P.; Martin, J. D. *J. Am. Chem. Soc.* **2001**, *123*, 7564−7573.

Table 2. Summary of the Crystallographic Data for the Ethylene Adducts of $CuAlCl_4$

formula	$(et)_2CuAlCl_4$		β-(et)$CuAlCl_4$	α-(et)$CuAlCl_4$
	single crystal	powder	single crystal	powder
formula weight	288.45	260.39	260.39	
temp, °C	−130	20	−173	20
space group	Pc (7)	$P2_1cn$ (33)	$Pna2_1$ (33)	$P2_1$
a, Å	7.1274(5)	7.2194(7)	7.306(2)	7.041(3)
b, Å	12.509(1)	12.658(3)	16.133(3)	10.754(8)
c, Å	11.997(3)	12.200(1)	7.094(1)	11.742(9)
β, °	91.19(1)			102.48(6)
V, Å^3	1069.3(3)	1114.8(2)	836.2(3)	868.1
Z	4	4	4	4
ρ_{calc}	1.792	1.718	2.068	1.988
λ, Å	0.71073 (Mo Kα)	0.93003	0.93760	0.92696
μ, cm^{-1}	3.06		3.897	
R	0.0352[a]	0.0312[c]	0.0809[a]	
R_w	0.0402[b]	0.0513[d]	0.2777[b]	

[a] $R = \sum||F_o| - |F_c||/\sum|F_o|$. [b] $R_w = \sum(|F_o| - |F_c|)^2/\sum|F_o|^2$. [c] $R_p = \sum|I_o - I_c|/\sum|I_o|$. [d] $wR_p = \sqrt{(M/\sum I_o^2)}$.

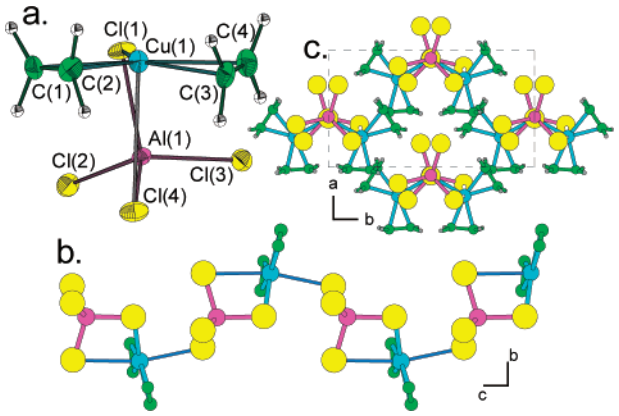

Figure 6. (a) ORTEP (50% probability ellipsoid) of **et-2**, viewed down the Cu(1)−Cl(4) axis emphasizing the psuedo-trigonal coordination of copper. (b) A ball-and-stick drawing highlighting the long axial copper-chloride contacts along the [001] direction (dark blue). (c) View looking down **c** showing the pseudo-close packing of the chlorine and ethylene.

The basic $(C_2H_4)_2CuAlCl_4$ molecular-type unit consists of a trigonal planar $(C_2H_4)_2CuCl$ fragment that is connected to a tetrahedral tetrachloroaluminate via chloride bridges, Figure 6a. The ethylene molecules are symmetrically coordinated to the copper in an η^2-fashion with the average ethylene-centroid to copper distance (Cu-et) of 2.03 Å. A summation of the centroid-Cu-centroid and centroid-Cu−Cl angles (359.9° and 359.7° for the crystallographicly distinct copper centers, respectively) emphasizes the planarity of the $(C_2H_4)_2CuCl$ unit. Each of the ethylenes is slightly twisted out of this molecular plane (et(1) 7.2(9)°, et(2) 1.9(1)°, et(3) 2.8(1)° and et(4) 9.2(1)°).

The di-ethylene copper chloride trigonal plane is strongly linked to the aluminum chloride unit by the bridging chlorine atom (Cu(1)−Cl(1) = 2.349(2) Å or Cu(2)−Cl(5) = 2.345(2) Å). A second, and much weaker intramolecular bridge through Cu(1)−Cl(4) = 3.125(2) Å or Cu(2)−Cl(7) = 3.163(2) Å is also observed, with this second bridging chloride occupying the apex of a pyramid below the trigonal plane, as illustrated in Figure 6a. In addition to these, a long intermolecular bridge to a chloride (Cu(1)−Cl(3) = 2.988(1) Å or Cu(2)−Cl(8) = 2.918(2) Å) in the apical position above the trigonal plane serves to link the molecular units into a 1-D chain. Although these long inter- and intramolecular Cu−Cl contacts are quite weak,

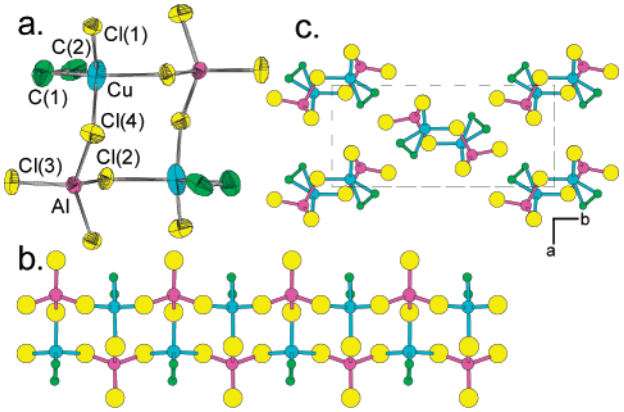

Figure 7. (a) ORTEP (50% probability ellipsoid) of the four-ring building block of **α-et-1** (b) A ball-and-stick drawing of the ladder chain running along the [010] direction. (c) A crystal-packing view looking down the chain axes.

their influence can be seen in the aluminum chloride distances, with the Al−Cl distances inversely correlated to the distance of the chloride to copper. Interestingly, when the crystal packing of these molecular-chain-type units is considered (Figure 6c), it becomes apparent that an ethylene ligand occupies a volume similar to that of a chlorine atom in the structure of $(C_2H_4)_2$-$CuAlCl_4$. A pseudohexagonal close packed sublattice is observed in which two ethylene molecules and one chloride make up the A-layer and the three basal chlorides of the tetrachloroaluminate tetrahedron make up the B-layer.

***β*-(et)$CuAlCl_4$, *β*-et-1.** The structure of ***β*-et-1** is best described as a ladder-type chain constructed of $(C_2H_4)CuAlCl_4$ rungs that are connected in an alternating sense along the 2_1 axis that runs down the center of the chain, parallel to the *c*-axis (Figure 7). To our knowledge, this is the first Cu(I)-ethylene complex with an extended structure. Each pair of ladder rungs creates a ring of four corner-shared tetrahedra with strict alternation of the copper and aluminum tetrahedra as shown in the ORTEP given in Figure 7a. In the low temperature crystal structure, the pairs of ladder-rungs within each four-ring are slightly displaced with respect to a center of inversion, consistent with the orthorhombic space group $Pna2_1$.

The ethylene is bound to the copper on the exterior of the ladder with a copper to ethylene-centroid distance of 1.96(1) Å. The ethylene molecule is coplanar with the Cu−Cl(2)−Al ladder rung (a mirror plane in the *Pnam* supergroup). The Cl(2) which forms the ladder rung also forms the strongest bridge between the copper and aluminum centers (Cu−Cl(2) = 2.348(3) Å, Al−Cl(2) = 2.181(3) Å). Orthogonal to the plane of the atoms in the rung, the copper atom is coordinated to the tetrachloroaluminate units of the rungs above and below to form the ladder scaffold with elongated copper chloride single bonds (Cu−Cl(1) = 2.569(4) Å and Cu−Cl(4) 2.557(5) Å). Quite contracted Cl−Cu−Cl bond angles (an average of 91°) are observed around the pseudo-tetrahedral $(C_2H_4)CuCl_4$ fragment resulting in a somewhat open coordination around the ethylene (centroid-Cu−Cl angles of 121° for Cl(1) and Cl(4) and 130° for Cl(2)). The variation in the strength of the Cu−Cl bridges is again manifest in the Al−Cl bond distances, which are inversely correlated to the Cu−Cl distances.

As viewed from the [001] direction in Figure 7c, these ladders pack with a herringbone pattern, a consequence of the **n**- and **a**-glide planes. Interestingly, like the structure of **et-2**, the

Table 3. ^{27}Al, ^{63}Cu, and ^{13}C NMR Parameters for **et-2** and **α-et-1**

	$(C_2H_4)_2CuAlCl_4$	α-$(C_2H_4)CuAlCl_4$
^{27}Al δ_{iso} (ppm) 25°C	102	102
QCC (MHz)	5.1	4.6
η	0.3	0.8
^{27}Al δ (ppm) 70 °C		101
^{65}Cu δ (ppm) 70°C		−300
^{13}C δ (ppm) 25 °C	109	105
^{13}C δ (ppm) 70 °C		106

structure of ***β*-et-1** is related to a pseudo-close packing of the chlorine and ethylene. The pseudo close-packed planes are parallel to the (010) plane. Within each layer of chains (in the ac plane), the central core consists of two layers, each composed of the three bridging chlorine atoms and the ethylene. These are approximately close-packed as A and B layers, respectively (albeit slightly elongated in the **a**-direction because of the van der Waals separation between chains). The terminal chlorides occupy B and A sites, respectively above and below this layer of chains giving a pseudo hexagonal close-packing of the ethylene and chlorine. However, the terminal chlorides from adjacent layers fill only half of the possible close packed sites at the junction between two layers of chains and thus are shifted out of registry along **a**. Nevertheless, this shift is such that the terminal chlorine atoms from adjacent layers are separated by only 3.66 Å. As a result, the cavity in which the ethylene sits in ***β*-et-1** is slightly larger than that observed for **et-2**.

α-(et)$CuAlCl_4$, α-et-1. Details of the structure of **α-et-1** remain elusive. Various attempts were made to solve the structure from synchrotron powder data for what is believed to be a >90% pure sample. All attempts yielded models which indicated a layered structure, somewhat reminiscent of the structure of $(C_6H_6)CuAlCl_4$.[27] The data also suggested the presence of four-rings (two copper and two aluminum tetrahedra) analogous to the pair wise rung structure of the ladder chains found in ***β*-et-1**. These structures were not, however, stable during the structure refinement and all yielded various chemically unreasonable atom−atom contacts. The best model for the structure, obtained to date, was obtained by using the $P2_1/c$ space group, and the structure is shown in Supporting Information Figure 3. However, the presence of a weak (001) reflection at 0.55 $Å^{-1}$ (Supporting Information Figure 4), indicates that the structure must adopt a lower symmetry $P2_1$ space group. Attempts to further refine this structure in the lower space group did not, however, result in any improvement in the goodness-of-fit. Nevertheless, these data seem to confirm the rigid-body characteristic of the $AlCl_4$ anion and the η^2-coordination of ethylene to the copper centers. This structural model is also consistent with the NMR data discussed below.

Multinuclear MAS NMR. Magic angle spinning (MAS) NMR experiments were performed to characterize the local environments of the different ethylene adduct phases and probe sorbent-sorbate interactions. ^{13}C ($I = {}^1/_2$, 99% enriched abundance), ^1H ($I = {}^1/_2$, 100% natural abundance) and the quadrupolar nuclei ^{27}Al ($I = {}^5/_2$, 100% natural abundance) and ^{63}Cu ($I = {}^3/_2$, 69% natural abundance) were used and the parameters extracted from these data are summarized in Table 3. $^{13}C/^{65}Cu$ TRAPDOR NMR (^{65}Cu, $I = {}^3/_2$, 31% natural abundance) was used for the first time to probe the binding of ethylene to copper-(I). MAS NMR experiments were conducted on a mixed α-$(^{13}C_2H_4)CuAlCl_4$/α-$CuAlCl_4$ sample, as well as a pure

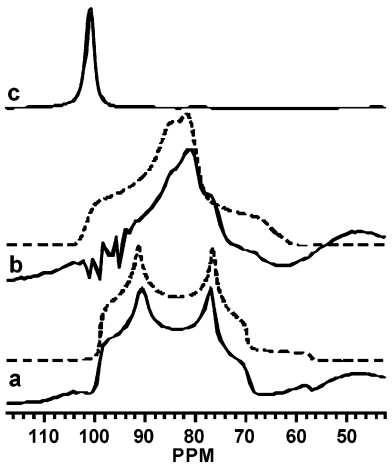

Figure 8. Experimental (solid lines) and simulated (dashed lines) ^{27}Al MAS NMR spectra of (a) **et-2** at 25 °C, (b) **α-et-1** at 25 °C (the ^{27}Al resonance at 97 ppm due to α-$CuAlCl_4$ has been subtracted from the experimental spectrum causing the distortion in the baseline at around 97 ppm) and (c) melt of **α-et-1** at 70 °C.

$(^{13}C_2H_4)_2CuAlCl_4$ sample. Variable temperature experiments were carried out to examine the α-$(^{13}C_2H_4)CuAlCl_4$/α−$CuAlCl_4$ sample up to 70 °C. The one-equivalent adduct used in the MAS NMR experiments was shown to be **α-et-1** and not ***β*-et-1** by placing the MAS sample holder directly into the synchrotron X-ray beam and collecting an XRD pattern.

^{27}Al MAS NMR. The room temperature ^{27}Al MAS NMR spectra of both **et-2**, and **α-et-1** (Figure 8), show central ($|+1/2> \rightarrow |-1/2>$) resonances that are broadened by the second-order quadrupolar interaction, accompanied by spinning sideband manifolds that spread over 1 MHz. The sidebands arise due to satellite transitions, which are affected to first-order by the quadrupolar interaction. Both **et-2** and **α-et-1** phases exhibit an isotropic ^{27}Al chemical shift at 102 ppm, which is consistent with literature values for the ^{27}Al MAS NMR of $AlCl_4^-$,[30,31] indicating that both contain $AlCl_4^-$ units. The center band of the **et-2** spectrum, at 85 ppm, consists of two distinct, well-separated discontinuities at 91 and 77 ppm. The center band of **α-et-1**, at around 80 ppm, contains two poorly resolved discontinuities at 85 and 81 ppm. The weaker peak at 104 ppm in both spectra is assigned to the isotropic resonance of the ^{27}Al $|\pm 3/2> \leftrightarrow |\pm 1/2>$ inner satellite transitions. The **α-et-1** spectrum (Figure 8.b) contains a weaker peak at 77 ppm, which is assigned to one of the discontinuities of the resonance due to **et-2**. A resonance due to residual α-$CuAlCl_4$ (97 ppm) was also observed, but this has been removed from the spectrum here by subtraction. Simulation of the central transition line shapes (the dashed lines in Figure 8) show a good fit to the experimental spectra, and provide values for the isotropic chemical shifts, δ_{iso}, quadrupolar coupling constants, QCC, and asymmetry parameters, η (Table 3). A small value for the asymmetry parameter, η of 0.3 is extracted for **et-2**. In contrast, the larger value η of 0.8 extracted for **α-et-1** indicates a more asymmetric local environment. The QCC's of the two adduct phases are large, 5.1 MHz for **et-2** and 4.6 for **α-et-1**. Second-order quadrupolar shifts for the central and inner satellite transitions are calculated to be approximately −16 and 2 ppm, respectively. These account for the observed shift in the center of gravity of the central transitions from the isotropic chemical shift value of 102 ppm to approximately 85 and 80 ppm, respectively, as

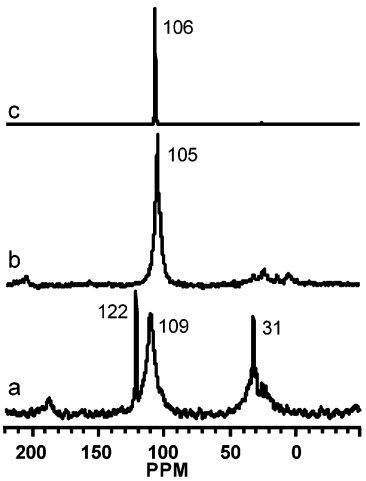

Figure 9. ^{13}C MAS NMR spectra (with ^{1}H decoupling) of (a) **et-2** at 25 °C, (b) **α-et-1** at 25 °C, and (c) melt of **α-et-1** at 70 °C.

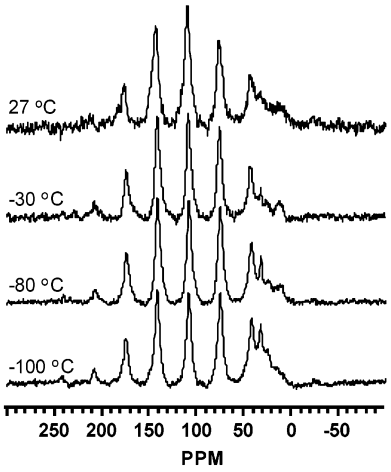

Figure 10. ^{1}H → ^{13}C CP MAS NMR spectra of **et-2** at decreasing temperatures (spinning speed = 3.0 kHz).

well as the shift of the isotropic resonance of the inner satellite transitions to 104 ppm.

The ^{27}Al MAS NMR spectrum of **α-et-1** acquired at 70 °C (Figure 8c) shows a strong, sharp resonance at 101 ppm, with no spinning sidebands, similar to that observed in the solution-phase ^{27}Al NMR spectrum of tetrachloroaluminate,[32] confirming that **α-et-1** has melted at this temperature.

^{63}Cu MAS NMR. The $I = 5/2$ nucleus ^{63}Cu is associated with a large quadrupole moment, which often results in extremely broad resonances for many Cu-compounds, particularly for Cu in distorted local environments. Nonetheless, we have previously reported spectra from both α- and β-$CuAlCl_4$.[30] Unfortunately, no signal could be detected in the ^{63}Cu MAS NMR spectra of either **et-2** or **α-et-1** at room temperature: in the spectrum of **α-et-1**, only a weak signal due to residual α-$CuAlCl_4$ was observed. The lack of signal from the two adduct phases is consistent with the low symmetry of the copper sites in the solid. At 70 °C, a broad ^{63}Cu resonance at approximately −300 ppm (Supporting Information Figure 5) is seen from the **α-et-1** melt; the rapid tumbling of the complex in the melt presumably resulting in a reduction in the quadrupolar broadening. There is a considerable uncertainty in the exact chemical shift of this resonance due to its exceptionally broad line width, approximately 25 kHz, and the amplitude of the baseline oscillation associated with the phasing of the signal.

^{13}C MAS NMR. The ^{13}C MAS NMR spectra of **et-2** and **α-et-1** at 25 °C are shown in Figure 9. A relatively broad resonance at 109 ppm and sharp resonances at 122 ppm and at 31 ppm (along with a few weak resonances between 20 and 40 ppm) are seen in the spectrum of **et-2**. The resonance at 109 ppm is assigned to ethylene in solid **et-2**, and the sharp peak just downfield at 122 ppm is assigned to free or physisorbed ethylene.[33] The upfield peaks at 31 ppm are tentatively assigned to oligomerized aliphatic products presumably in the liquid state. The amount of oligomerized product is sample dependent, and does not change significantly over-time even when the adduct is heated to 70 °C. Thus, this oligomerized product likely results from traces of moisture that are stoicheiometrically consumed in the reaction. The spectrum of **α-et-1** shows a resonance at 105 ppm, which is assigned to bound ethylene in the solid. Small sharp resonances at around 23 ppm are ascribed to aliphatic oligomers. Spinning sideband manifolds over 12 kHz wide due to combination of ^{13}C chemical shift anisotropy and ^{13}C−^{13}C dipolar coupling are observed for the resonances of both ethylene adducts in the slow spinning spectra, indicating that ethylene is rigidly bound in **et-2** and **α-et-1** at 25 °C. The spinning sideband manifold collapses and an intense, sharp resonance is seen at 106 ppm in the spectrum of the melted ethylene adduct at 70 °C (Figure 9c).

Variable temperature ^{1}H → ^{13}C CP MAS NMR spectra of **et-2**, acquired at spinning speed of 3.0 kHz, are displayed in Figure 10. At 27 °C, the spectrum is dominated by the resonance at 109 ppm; the weaker resonances at approximately 31 ppm are due oligomers. At lower temperatures, the spinning sideband intensity increases relative to the intensity of the central band, and the oligomer signal also increases. At temperatures below about −80 °C, the first-order spinning sidebands become stronger than the central band, giving rise to a "Pake-Doublet"-like sideband pattern, which is ascribed to ^{13}C−^{13}C homonuclear coupling. This suggests that ethylene motion is not completely frozen at room temperature and that lowering the temperature down to −120 °C reduces ethylene mobility. The oligomer signal is also enhanced at low temperature presumably due to an enhancement in CP efficiency as the oligomers become rigid.

Even though the ^{63}Cu or ^{65}Cu NMR spectra are not directly observable, the ethylene binding can be probed with a ^{13}C/^{65}Cu TRAnsfer of Populations in DOuble Resonance (TRAPDOR) NMR method.[34] In this experiment, the intensity of a ^{13}C MAS echo signal due to ^{13}C nearby Cu will decrease on applying ^{65}Cu irradiation during the evolution period of the echo sequence. Figure 11 displays the ^{13}C/^{65}Cu TRAPDOR NMR control, double resonance and difference spectra for **et-2** at −80 °C. A TRAPDOR fraction of approximately 20%,

(31) (a) Schurko, R. W.; Wasylishen, R. E.; Phillips, A. D. *J. Magn. Reson.* **1998**, *133*, 388−394. (b) Han, O. H.; Oldfield, E. *Inorg. Chem.* **1990**, *29*, 3666−3669. (c) Akitt, J. W. *Prog. Nucl. Magn. Reson. Spectrosc.* **1989**, *21*, 1−149.

(32) (a) Kidd, R. G.; Truax, D. R. *J. Am. Chem. Soc.* **1968**, *90*, 6867−6869. (b) Deroault, J.; Granger, P. Forel, M. T. *Inorg. Chem.* **1977**, *16*, 3214−3218. (c) Wilinski, J.; Kurland, R. J. *J. Am. Chem. Soc.* **1978**, *100*, 2233−2234.

(33) Beeler, A. J.; Orendt, A. M.; Grant, D. M.; Cutts, P. W.; Michl, J.; Zilm, K. W.; Downing, J. W.; Facelli, J. C.; Schindler, M. S.; Kutznelnigg, W. *J. Am. Chem. Soc.* **1984**, *106*, 7672−7676.

(34) (a) Grey, C. P.; Vega, A. J. *J. Am. Chem. Soc.* **1995**, *117*, 8232−8242. (b) Grey, C. P.; Kumar, B. S. Arun. *J. Am. Chem. Soc.* **1995**, *117*, 9071−9072.

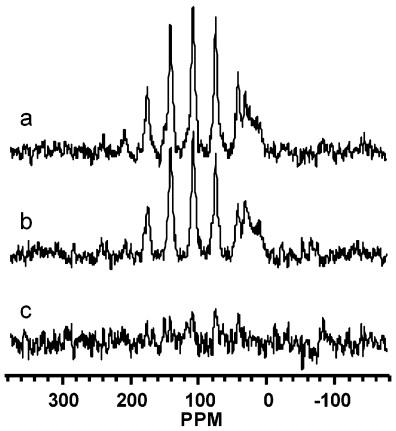

Figure 11. $^{13}C/^{65}Cu$ TRAPDOR NMR of **et-2** at −80 °C; (a) control, (b) double resonance, and (c) difference spectra.

calculated from comparison of the echo magnitudes of the two FID's, is found for the 109 ppm resonance, whereas no TRAPDOR effect is seen for the oligomer resonances. This is most clearly demonstrated by the difference spectrum (Figure 11c). On the basis of the natural abundance of ^{65}Cu (31%), a maximum possible $^{13}C/^{65}Cu$ TRAPDOR fraction of no more than 31% is predicted. In addition, the very large ^{65}Cu QCC and the low power of ^{65}Cu irradiation frequency (due to the poor isolation of the ^{13}C and ^{65}Cu channels and the closeness in the two Larmor frequencies) will further reduce the size of the TRAPDOR fraction.[34] Residual motion of ethylene, and thus reduced $^{13}C-^{65}Cu$ dipolar coupling, would further suppress the TRAPDOR effect. Therefore, an observed TRAPDOR fraction of 20% is consistent with a strong $^{13}C-^{65}Cu$ dipolar coupling and ethylene-copper binding.

Diffuse Reflectance UV−Vis Spectroscopy. The electronic structure of the copper (I) tetrachloroaluminate ethylene adducts was probed with variable pressure diffuse reflectance UV−vis spectroscopy. Figure 12a follows the stepwise increase in the ethylene pressure over a sample under conditions that are close to the early portion of the volumetric adsorption experiment in Figure 1 curve 100-a. Upon sorption of ethylene, a strong peak at 32×10^3 cm^{-1}, with a greater molar absorptivity than the starting material, grows in and dominates the spectrum. A broad absorption feature at 44×10^3 cm^{-1} is also observed. Equivalent spectra were obtained from several reactions, but it is not currently possible to determine whether this spectrum corresponds to the **α-** or ***β*-et-1** polymorph. In a second experiment (Figure 12b), a sample of α-$CuAlCl_4$ was exposed to 1500 Torr of ethylene to form **et-2**. The sample of **et-2** was then exposed to a dynamic vacuum while monitoring the change in the absorption spectrum. The initial spectrum (top), assigned as an essentially pure sample of **et-2** consists of three strong sorption features at 32×10^3 cm^{-1}, 36×10^3 cm^{-1} and 48×10^3 cm^{-1}. Upon desorption, the two higher energy absorption bands rapidly diminish in intensity, whereas the band at 32×10^3 cm^{-1}, that is common to the one-equivalent adduct phase, is observed to persist, albeit at lowered intensity. Analogous to both the adsorption isotherm and time/pressure resolved diffraction measurements, complete desorption of the ethylene adduct to $CuAlCl_4$ is not observed at room temperature. Nevertheless, placing this desorbed sample under a hand-held UV lamp with 254 nm excitation, the characteristic blue luminescence of

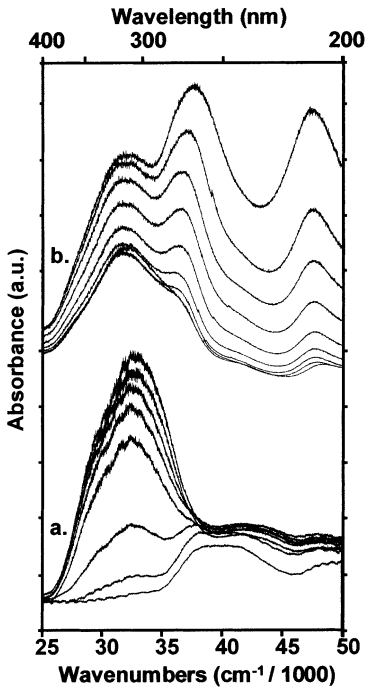

Figure 12. Diffuse reflectance UV−visible spectra of (a) α-$CuAlCl_4$ exposed to ethylene pressure of 7.1 Torr, 23.7 Torr, 77.1 Torr, 109.7 Torr, 180.8, 475.7, and 954.0 Torr demonstrating the formation of **α-et-1** and (b) the desorption of ethylene from **et-2** under dynamic vacuum for 0, 8, 16, 24, 32, 40, and 480 min, respectively.

Scheme 1

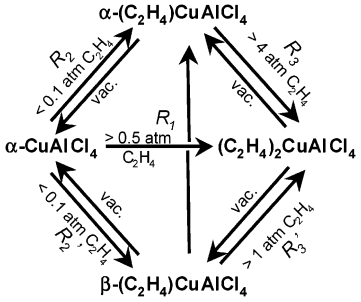

$CuAlCl_4$ is observed,[35] consistent with a mixture of α-$CuAlCl_4$ and **α-et-1**.

Discussion

The diffraction, adsorption isotherm and spectroscopic results presented in this paper implicate a complex set of reaction pathways involved in the remarkable ability of $CuAlCl_4$ to reversibly sorb up to 200 cm^3 of ethylene relative to stp (0.24 g) per gram of $CuAlCl_4$ at ethylene pressures well below ambient. These reaction pathways are summarized in Scheme 1. Much of this solid−gas reactivity can be traced to significant features of the $CuAlCl_4$ lattice. Thus, we begin this discussion with a description of the salient features of the parent crystal lattice. The structural and spectroscopic measurements of the adduct phases provide a clear picture of the comparative olefin binding and also suggest further possible reactivity. Finally, by consideration of all the sorption data and discerning analogous structural features between the parent and adduct structures, we propose an atomistic model for the mechanism of these reactions.

(35) Sullivan, R. M.; Martin, J. D. *J. Am. Chem. Soc.* **1999**, *121*, 10 092−10 097.

Structure and Bonding. Though not a microporous material, $CuAlCl_4$ has the capacity to sorb large quantities of ethylene by a process that we describe here as sorptive reconstruction. This sorptive process requires a relatively soft and/or flexible crystal lattice, and, an olefin binding affinity that is sufficient to break up the parent crystal lattice. At the same time, for this process to be reversible, the olefin must not be bound so tightly that it cannot be removed and the reassembly of the parent network must also be facile. We previously described the lattice of α- and β-$CuAlCl_4$ and noted that whereas the chlorine atoms adopt an approximately close-packed sublattice, a 2×2 zigzag chain type filling of 1/4 of the tetrahedral interstices with Cu^I and Al^{III} cations creates several types of van der Waals channels.[28] Although these van der Waals channels, exhibiting a free diameter of only 0.5 Å, are too small for molecular diffusion, they may play an important role in directing the path for ethylene penetration into the lattice. It is likely that the $AlCl_4^-$ tetrahedra are the most robust structural unit throughout the framework reconstruction process. In the single-crystal structures of ***β*-et-1** and **et-2**, the average Al−Cl distances are equivalent to those observed in the parent α- and β-$CuAlCl_4$ phases. Similarly, the ^{27}Al chemical shifts, $\delta_{iso} = 102$ ppm, are identical in the one- and two-equivalent ethylene adducts, and these are very similar to the values of 97 ppm observed for both α- and β-$CuAlCl_4$[30] and 100 ppm for $NaAlCl_4$.[31b] Furthermore, the phase transition from β- to α-$CuAlCl_4$ was shown to proceed with libration of intact tetrachloroaluminate units along with migration of the cuprous cations.[30] By contrast, the mobility of the Cu^I centers along with the known propensity of Cu^I to undergo second-order Jahn−Teller distortions[36] allows the copper center to adopt a variety of coordination geometries making it the likely site for the ethylene coordination.

In each of the three olefin adduct phases, the ethylene molecules are bound to copper in an η^2-coordination mode. The olefin to copper distances are slightly shorter in the one equivalent adduct, ***β*-et-1** = 1.96(1) Å, than in the two equivalent adduct, **et-2** = 2.03(1) $Å_{(ave)}$. The desorption isotherms for the one- and two-equivalent ethylene adducts are consistent with the correlation between bond-lengths and bond-strength. In the inset of Figure 2, it is observed that ethylene begins to desorb from **et-2** at about 50 Torr, whereas **et-1** does not begin to desorb ethylene until below 10 Torr. Nevertheless, the C−C distances in both crystalline structures are 1.34 Å, equivalent to that of free ethylene. The ethylene ligand fills one of the pseudo tetrahedral copper coordination sites in the β-one-equivalent adduct. Though described as pseudo-tetrahedral, the acute Cl−Cu−Cl bond angles, with the olefin coordinated parallel to the base of the $CuCl_3$ trigonal pyramid increases the σ-type overlap between the empty copper sp-orbital and the olefin π-bond. The rotational orientation of the olefin is stabilized by a weak back-bonding interaction into the olefin π*-orbital. In the two-equivalent adduct, the two olefin ligands are coplanar with the copper and one Cl ligand giving a geometry consistent with other copper diolefin complexes and reminiscent of the structure proposed for $Ni(et)_3$.[37] The planar coordination of the olefins is stabilized by weak π-back-bonding. Interestingly, this coordination geometry places the inner carbons of the two ethylene ligands at a separation of only 3.13(1) Å, which is almost 0.2 Å less than the sum of their van der Waals radii. This coplanar olefin coordination geometry may contribute to the previously reported catalytic formation of linear ethylene oligomers.[26]

The ^{13}C NMR data further demonstrate the similarity in bonding between the one- and two-equivalent adducts, and also highlight the influence of the ancillary ligands on the copper-olefin coordination. It has previously been shown that the ^{13}C chemical shift of vinyl carbons in olefins bound to Cu^I is quite sensitive to the extent of π-back-bonding, but that both σ- and π-interactions result in an upfield shift with respect to free ethylene.[38] Here, the ^{13}C chemical shifts of 109 and 105 ppm for **et-2** and **α-et-1**, are shifted upfield by 14 and 18 ppm, respectively, with respect to free ethylene. This shift is comparable to the upfield shift observed for olefins bound to Cu^I with a triflate counterion.[38] By implication, the $AlCl_4^-$ anion, the conjugate base to the strong Lewis acid $AlCl_3$, yields a Cu^I coordination environment with a similar Lewis acidity to that of triflate complexes. Here, any copper-olefin π-interaction is negligible, but the strong σ-olefin complex results in the upfield shift. The 4 ppm greater upfield shift of **α-et-1** with respect to **et-2** is consistent with a slightly stronger copper-olefin bonding in the one-equivalent adduct. By way of comparison, in the presence of strong donor ligands such as in the bioinorganic model complexes $[Bu^t_2P(NSiMe_3)_2N]Cu(et)$ and $[HB(3\text{-}(CF_3),5\text{-}(R)Pz]Cu(C_2H_4)$ (R = H, C_6H_5, and CF_3), the Cu^I centers are less Lewis acidic thus exhibit significant π-back-bonding resulting in chemical shifts upfield from free ethylene by 50, 38, 38, and 34 ppm, respectively.[9g,h] These data, along with our observations that higher pressures are required for ethylene to bind to $CuGaCl_4$ and that no ethylene was bound to $CuAlBr_4$ at pressures below 1500 Torr, as well as the previously reported weak binding of ethylene to CuCl[19] begin to map out a similar Lewis acid controlled binding of ethylene to Cu(I) as was previously articulated for nonclassical vs classical carbonyl complexes.[15] Here, nonclassical olefin complexes are formed when σ-type binding is favored by a coordination environment that is more Lewis acidic than chlorine, and classical olefin complexes are formed when π-type binding is favored by ligands that are more Lewis basic than chloride.

The UV−vis spectra of the ethylene adducts provide a picture of the electronic structure of these materials and point toward an anticipated further reactivity. The electronic structure of the parent $CuAlCl_4$ has been previously described, with the lowest energy transition (40×10^3 cm^{-1}) resulting from the copper centered $3d^{10}$ to $3d^94s^1$ transition.[35,39] Upon reaction with ethylene, the lower energy transition observed to grow in at 32×10^3 cm^{-1}, as seen in Figure 12a, is a MLCT transition; a result of the insertion of the olefin π*-orbital into the metal-based HOMO/LUMO gap. By way of comparison, the lowest energy π to π* absorption in free ethylene is 61×10^3 cm^{-1}.[40] The weaker absorption due to the metal-centered transitions is shifted to slightly higher energy (44×10^3 cm^{-1}) consistent with the π-stabilization and σ-destabilization of the copper 3d, and 4s and 4p orbitals, respectively, upon olefin binding.

(36) Burdett, J. K.; Eisenstein, O. *Inorg. Chem.* **1992**, *31*, 1758−1762.
(37) Fisher, K.; Jonas, K.; Wilke, G. *Angew. Chem., Int. Ed.* **1973**, *12*, 565−567.
(38) Salomon, R. G.; Kochi, J. K. *J. Organometallic Chem.* **1974**, *64*, 135−143.
(39) Texter, J.; Strome, D. H.; German, R. G.; Klier, K. *J. Phys. Chem.* **1977**, *81*, 333−338.
(40) Jones, L. C.; Taylor, L. W. *Anal. Chem.* **1955**, *27*, 228−237.

Because of the similarity in olefin bonding between them, there is no discernible shift in the λ_{max} of metal-to-ligand absorption between the one- and two-equivalent ethylene adducts, although it becomes significantly more intense for the two equivalent adduct. The spectrum of **et-2** is dominated by two new absorption features at 36×10^3 cm^{-1} and 48×10^3 cm^{-1}, assigned to metal-centered transitions. The structural transformation from the pseudo-tetrahedral geometry of the one-equivalent adduct to the pseudo trigonal-planar geometry of **et-2** results in a significant rehybridization of the metal-based orbitals. The p_z-orbital (as defined with the *z*-axis orthogonal to the $(et)_2CuCl$ plane) has no symmetry match with the in-plane ligands, and thus this low-lying nonbonding orbital gives rise to the new absorption feature at 36×10^3 cm^{-1}. This orbital is only weakly destabilized by the long axial Cu−Cl contacts that bridge to the Al. Since the $AlCl_3$ is a much stronger Lewis acid than Cu^I, it competes much more effectively for the bonding to chlorine. The higher energy feature at 48×10^3 cm^{-1} is assigned to the copper centered d to s/p transition.

It is further interesting to note that this nonbonding LUMO of **et-2** is at lower energy than the LUMO of the parent $CuAlCl_4$ suggesting that the two-equivalent adduct may be susceptible to further nucleophilic attack. This low lying, empty orbital may also be a key to the observed reactivity of $CuAlCl_4$ as a cocatalyst with alkyl-aluminum species in the formation of low molecular weight ethylene oligomers.[26] Such low molecular weight oligomerization catalyzed by a transition-metal complex in the presence of aluminum alkyls, also observed for the isoelectronic and nearly isostructural $Ni(et)_3$ (the said "nickel effect"), is unusual for transition-metal catalyzed polymerizations which tend to form higher molecular weight oligomers.[41] This low-lying LUMO may also play a role in the low barrier to ethylene diffusion through **et-2**.

Mechanistic Considerations. The reaction scheme proposed in Scheme 1 suggests that there are multiple reaction paths that lead to the same **et-2** product. The dramatic difference in ethylene sorption between the high-pressure and low-pressure experiments seem to imply that there may be a direct path to **et-2**, accessible only with the higher ethylene concentrations, and there appears to be a kinetic barrier preventing the one-equivalent adducts from forming the two-equivalent phase. This raises the question as to whether it is necessary to go through a one-equivalent intermediate to form the two-equivalent adduct? Or is there a direct path from $CuAlCl_4$ to **et-2**?

To begin to probe these mechanistic questions, we simplify our consideration to only the adduct formation reactions in Scheme 1. Observation of the intermediate phases **α-et-1** and ***β*-et-1** in the time/pressure resolved diffraction measurements demonstrates that the rate of formation of **et-2** from the one-equivalent adducts, **et-1**, is the slow step under low-pressure reaction conditions (i.e., $R_2 > R_3$ and $R_2' > R_3'$). Furthermore, if a direct route R_1 exists, then under low-pressure conditions, $R_2 \gg R_1$. If under higher-pressure conditions, R_3 (or R_3') became fast with respect to R_2 (or R_2') then the intermediate one-equivalent adduct would not be observable, thus giving the appearance of a direct route from α-$CuAlCl_4$ to **et-2**. However, when both α-$CuAlCl_4$ and **et-1** are exposed to 1500 Torr of ethylene pressure, the former reaction exhibits rapid and complete formation of **et-2** whereas the latter reaction exhibits only incomplete formation of **et-2**. This suggests that in fact there is a direct path, R_1, for the formation of **et-2** from $CuAlCl_4$. The existence of a direct reaction path for the formation of **et-2** is further supported by the isobestic character of the diffractogram of Figure 4a, in which the cut immediately following the exposure to 1500 Torr of ethylene exhibits the diffraction pattern for both α-$CuAlCl_4$ and **et-2**, but there is no evidence for either intermediate phase. This experiment does not preclude the presence of an amorphous phase. Because desorption of ethylene should be disfavored at higher pressures, it is also reasonable to rule out the possibility that **et-2** formed from **et-1** proceeds by desorption of ethylene from **et-1** followed by resorption of two equivalents via the R_1 path. Rather **et-2** formed from **et-1** proceeds by R_3 (or R_3').

It is not yet clear what factors favor the formation of **α-et-1** over ***β*-et-1**. Diffraction measurements have shown the formation of both phases upon ethylene sorption into α-$CuAlCl_4$ and upon desorption from **et-2**. Experiments run at temperatures ranging from 15 °C to 35 °C give no indication that the temperature of the reaction gives a preference for one or the other product. The best correlation to date seems to be a qualitative observation that opening the capillaries to mount them on the gas-line goniometer under more humid conditions increases the likelihood that the ***β*-et-1** phase will be observed. It is possible that the trace moisture could create a different set of nucleation sites that favor the formation of ***β*-et-1**, than are present in the anhydrous reactions that seem to favor **α-et-1**. Also as noted above, ***β*-et-1** was the only adduct-phase observed in the reaction of ethylene with *β*-$CuAlCl_4$, although this reaction has not been repeated frequently enough to confidently state that the **α-et-1** adduct is never formed from *β*-$CuAlCl_4$. We thus hypothesize that the growth of a particular one-equivalent phases from α-$CuAlCl_4$ is controlled by differential nucleation.

The difference in the transport of ethylene through the respective $CuAlCl_4$, **α-et-1**, ***β*-et-1** and **et-2** phases must play a significant role in directing the various reaction pathways. Because reaction of ethylene with $CuAlCl_4$ readily and completely forms **et-1** at low-pressure, and **et-2** from high-pressure reactions, it is reasonable to propose that the transport of ethylene through α-$CuAlCl_4$ is facile, and, that growth at the phase-boundaries are the rate-limiting components of these reactions. By contrast, the gradual formation of **et-2** from **et-1** in the isotherms of Figure 1 (100-a, 50, and 30) and the UV−vis isotherm of Figure 12, for example, suggests a significant barrier to diffusion through the one-equivalent phase. We speculate that the difference between the isotherms of Figure 1 100-a and 100-b is that **α-et-1** is formed in the former, whereas ***β*-et-1** is formed in the latter. If this is the case, then a more facile ethylene transport through ***β*-et-1** could be responsible for the formation of **et-2** at lower pressures in reaction 100-b than in 100-a. We are currently measuring the reaction kinetics to probe these diffusion and growth models.

Comparative Analysis of Crystal Structures. A comparative analysis of the parent and adduct crystalline structures, along with the mechanistic details articulated above, begins to present an atomistic view of the reaction pathways for these sorptive reconstruction reactions. The van der Waals channels through the parent phases provide a first clue to significant structural analogies with the adduct phases. Both the α- and *β*-phases of

(41) Fischer, K.; Jonas, K.; Misbach, P.; Stabba, R.; Wilke, G. *Angew. Chem., Int. Ed.* **1973**, *12*, 943−1026.

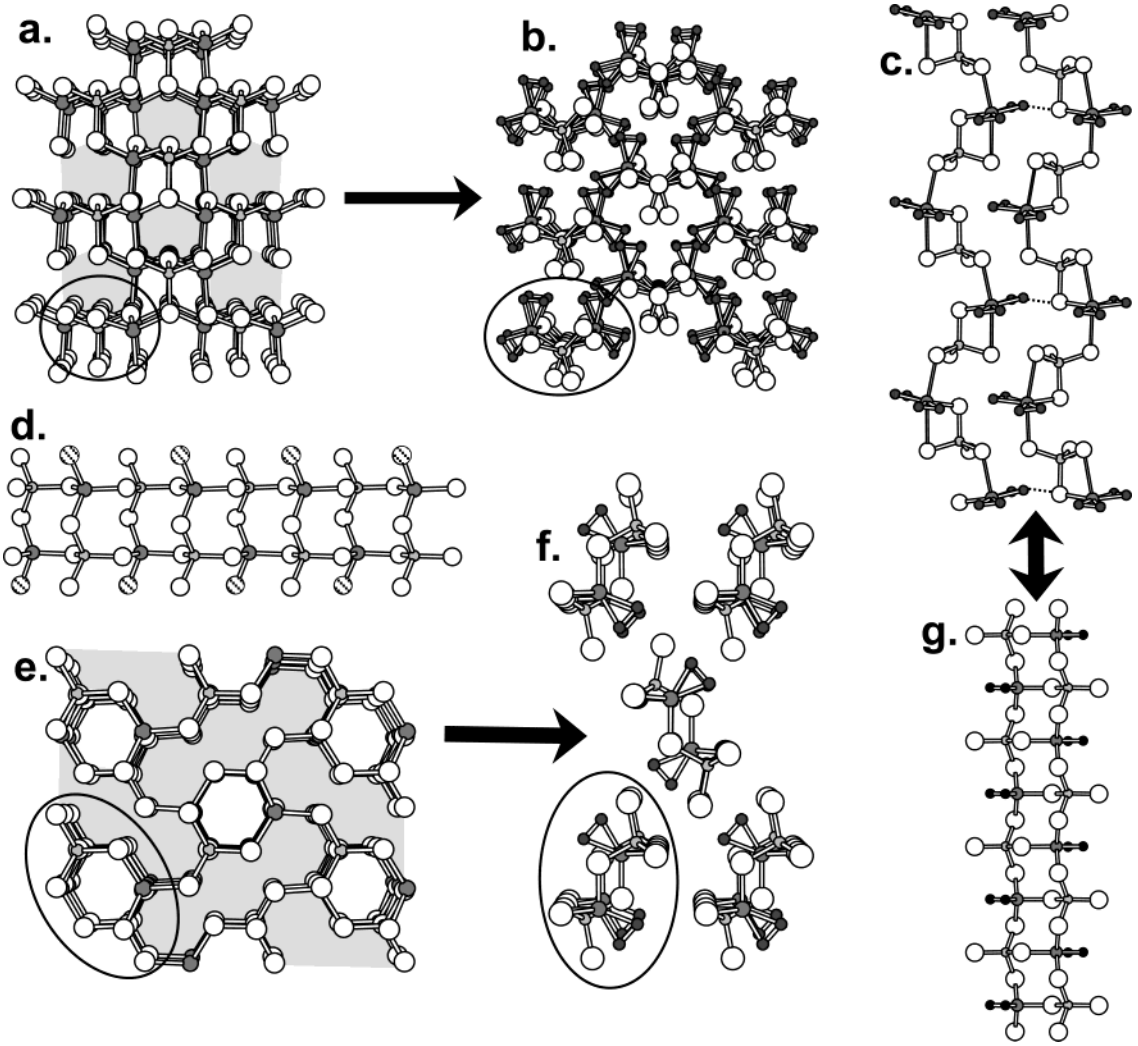

Figure 13. (a) View of α-$CuAlCl_4$ down the 112 vector. One zigzag chain is circled and the openings to the van der Waals channels are shaded. (b) Crystal packing view of **et-2** looking down the **c** axis. (c) Pair of adjacent chains in **et-2** with dashed lines highlighting the closest ethylene to Cl contacts. (d) View of a chain excised from β-$CuAlCl_4$ running parallel to the **c** axis. (e) View of β-$CuAlCl_4$ looking down the **c** axis. The openings to the *hcp* van der Waals channels are shaded, and one chain-precursor is circled. (f) Crystal packing view of ***β*-et-1** looking down the **c** axis. (g) One ladder chain of ***β*-et-1**.

$CuAlCl_4$ share an analogous set of close-packed van der Waals channels created by the separation between 2 × 2 zigzag chains, Figure 13a.[28] Because α-$CuAlCl_4$ adopts a cubic-close-packing there are four sets of these channels running parallel to the set of [1,1,2] lattice vectors. By contrast, β-$CuAlCl_4$ exhibits hexagonal-close-packing, and thus there is only one such set of channels which runs parallel to **a**. Remarkably a similar, but elongated set of 2 × 2 chains is observed in the structure of **et-2**, Figure 13, parts b and c. The similarity of these structures is highlighted by comparison of the views of α-$CuAlCl_4$ and **et-2** looking down the respective chains, Figure 13, parts a and b. A notable difference between the parent and adduct chains is that in the ethylene adduct, the copper atoms are pulled to the opposite side of the chloride plane than the aluminum atoms. It is thus reasonable to propose that this reaction proceeds by a classic S_{N2}-type backside attack by ethylene on the copper site. As an ethylene-copper bond is formed, there is an inversion of configuration at the copper center resulting in the cleavage of the copper−chlorine bond that is trans to the site of attack. Two such backside-attacks with inversion at each copper center completely excise these chains. Although it is unlikely that the binding of the two molecules of ethylene is concerted, in this reaction the binding of the second equivalent is apparently faster than the binding of the first equivalent such that no intermediate is observed.

A similarly strong structural correlation is observed between the structures of β-$CuAlCl_4$ and ***β*-et-1**, Figure 13d−g. Excision of the chains separated by the *hcp*-van der Waals channels of β-$CuAlCl_4$, Figure 13e, yields the ladder chain of Figure 13d, which is remarkably similar to the ladder chain of ***β*-et-1**, Figure 13g. The penetration of ethylene into the *hcp*-channel with an associative exchange of ethylene for the chlorine bound to the copper centers, and loss of the copper−chlorine bond syn to the site of attack, can be readily envisioned to account for this excision process. The cubic-close-packing of the 2 × 2 zigzag chains in α-$CuAlCl_4$ blocks the direct structural analogy to the ***β*-et-1** phase. Nevertheless, a similar cut of the lattice perpendicular to the close-packed planes show that a precursor to the ***β*-et-1** ladder chain exists with every other pair of rungs in the ladder expanded.

Such structural analogies between parent and adduct phases also lend support to the working structural model of the **α-et-1** phase based on attempted powder refinements. The model structure of **α-et-1** can be obtained upon excision of α-$CuAlCl_4$

by the two-dimensional penetration of ethylene through the tetragonal set of van der Waals channels as shown in Figure 6 of supplemental information.

Finally, we note the high structural correlation between the ladder-chain of ***β*-et-1**, Figure 13g, with a pair of neighboring chains of **et-2**, Figure 13c. For each pair of chains of **et-2** there are reasonably close contacts between every fourth ethylene ligand and a chlorine ligand from a neighboring chain (C−Cl = 3.76 Å), highlighted with dotted lines in Figure 13c. It is thus possible to envision that a S_{N2}-type sorptive scission converts ***β*-et-1** to **et-2** and that desorption of **et-2** to ***β*-et-1** proceeds with a zipper-type reconstruction upon ethylene loss via a dissociative substitution mechanism. The additional reconstruction required because of the apparent 2-D network in **α-et-1** may account for the apparently larger barrier to formation of **et-2** than is observed from the parallel chains of ***β*-et-1**.

Conclusion

The reversible binding of ethylene to copper aluminum chloride has been characterized by single crystal and powder X-ray diffraction, ^{13}C, ^{27}Al, and ^{63}Cu NMR and diffuse reflectance UV−vis spectroscopy as well as by gravimetric and volumetric adsorption analysis. The three novel adduct phases provide the first structural descriptions of ethylene binding to copper (I) in the presence of Lewis acids. The binding of ethylene to $CuAlCl_4$ provides a strong parallel to the nonclassical binding of CO to metal complexes.[15] Cu connected to the conjugate base of a strong Lewis acid (i.e., $AlCl_4^-$) is incapable of any significant π-back-bonding, but the lowered empty s,p-orbitals make the copper center a very good σ-acceptor. The structure of the approximately trigonal planar two-equivalent ethylene adduct causes a further electronic reorganization such that one Cu 3p orbital becomes effectively nonbonding, and thus is of lower energy than the LUMO of the parent material. These demonstrate the control of both the coordination environment and the complex geometry on the reactivity of the system.

The remarkable solid-state sorptive reconstruction of $CuAlCl_4$ upon ethylene sorption/desorption provides a dramatic challenge to the common perception of crystalline solids as rigid lattices, but also demonstrates the commonality of reaction mechanisms in solid-state and molecular chemistry. The flexibility of this crystalline solid allows for the sorption of large quantities of olefins. Reconstruction of the crystalline framework upon sorption/desorption appears to be directed by the symmetry and dimensionality of the van der Waals channels that penetrate the condensed crystalline framework. This sorption process, in which molecules that are an order of magnitude larger than any channels in the lattice are reversibly sorbed into the crystalline network, can figuratively be envisioned as an analogue to a rat snake swallowing an egg. To swallow the large object, the snake disengages its jaw, creating the larger opening. Here, the unlocking of the "mouth" of the van der Waals channel appears to proceed by a classic S_{N2}-type substitution reaction. The nucleation event(s) apparently control which channels are opened and thus which of the three adduct phases are formed. Further measurement of the kinetics of these reactions will be necessary to decipher the nucleation and growth components of these reactions. Nevertheless, based on the correlation between their crystal structures, we suspect that it will be possible to correlate the dimensionality of the crystal growth rate laws with the 1-D, 2-D, or 3-D sets of van der Waals channels that relate the parent and adduct phases.

Experimental Section

General Methods and Materials. All manipulations were performed under an inert atmosphere in a Dry-Box or using Schlenk or vacuum lines. The ternary halides α- and *β*-$CuAlCl_4$, α-$CuAlBr_4$, and α-$CuGaCl_4$ were prepared according to literature methods.[28] Ethylene gas of natural isotopic abundance was used as purchased from Specialty Gas for the time-resolved PXRD, gravimetric and barrometric experiments. Double ^{13}C-labeled ethylene gas, was purchased from Cambridge Isotopes. The ethylene for *ex situ* loaded MAS NMR samples was further purified by fractional condensation.

Adsorption Isotherm Measurements. Gravimetric measurements were carried out in a tared Pyrex Schlenk tubes, loaded with α-$CuAlCl_4$ and a predetermined pressure of N_2. After determining the total mass, the tube was evacuated and the loaded with C_2H_4 of at the same predetermined pressure. Because the molecular weights of N_2 = 28.0 g/mol and C_2H_4 = 28.0 g/mol are equivalent, an equal number of moles of gas are present in a given volume at a given pressure. Thus any measured difference in mass upon substituting N_2 with C_2H_4 corresponds to the C_2H_4 sorbed by the $CuAlCl_4$. In a typical experiment, 0.5 g of α-$CuAlCl_4$ exhibited an increase in mass by 0.12 g within 2 h when exposed to 1500 Torr of C_2H_4, and no further sorption over the following twenty hours. The heat of the reaction is frequently observed to partially melt the material giving the appearance of a "wet" solid at compositions intermediate between the two solid adduct phases; characteristic of a eutectic-type behavior. The melt behavior during the course of the sorption reaction can be prevented by cooling the sample to approximately 15 °C at which temperature the material remains crystalline throughout the entire sorption and desorption cycle.

Adsorption isotherm measurements were performed using a stainless steel volumetric gas/vacuum line constructed using 1/4 in. tubing and Swage Lock connectors (line volume = 40.25 mL). Both manual and pneumatic Nupro valves were used to control the atmosphere of the line and the system was automated using LabView software. The pressure of the system was measured with an MKS Baratron 690A pressure transducer (0.01 Torr to 5000 Torr, ±0.12%). In a glovebox powdered samples (40−50 mg) were dispersed across the 2 cm^2 base of a Pyrex sample holder, which was enclosed in a 26 mL stainless steel container. The sample container was affixed to the gas line with Swage Lock connectors. The dead-volume of the sample holder was measured with an N_2 isotherm. The calibrated volume of the gas line was filled with a predetermined dosing pressure, then the valve to the sample holder was opened, and the gas was allowed to expand into the sample volume. Samples were exposed to various initial ethylene pressures and to varying ethylene doses, so as to step the pressure in 30, 50, 100, 200, and 300 Torr steps. Exposure pressures and step sizes were metered with respect to the line pressure, but expansion to the line + sample volume results in reduced pressures. For example, in the 100-a sorption isotherm (Figure 1) the initial line pressure of 103 Torr reduced to 62 Torr upon expansion into the previously evacuated sample volume. This initial exposure pressure equilibrated to 15 Torr after 30 min corresponding to the sorption of 0.7 molar equivalents of ethylene by $CuAlCl_4$. In subsequent steps, 100 Torr of ethylene above the equilibrated pressure was added to the line, which, when expanded to the line + sample volume corresponded to a 14 Torr step for the second aliquot and approximately 60 Torr steps thereafter. (Data for Figure 1 100-c and Supporting Information Figure 1 100 were obtained using a different gas line V_{line} = 13.28 mL and V_{sample} = 17 mL.)

Time/Pressure Resolved Powder X-ray Diffraction. Powder X-ray diffraction experiments were performed at the X7B beamline of the National Synchrotron Light Source at Brookhaven National Laboratory with a wavelength of approximately 1 Å, in a Debye−Scherrer collection geometry, using either a translating image plate (TIP) detector

mounted on a four circle Huber diffractometer,[42] or a *MAR345* Image Plate Detector System. The TIP detector provides 30−40 s time resolution by exposing only a radial slice of the full Debye−Scherrer rings to a translating image plate, but is particularly subject to preferred orientation effects as the crystallite size, orientation, and distribution changes during the course of the reaction. By contrast the MAR detector collects a full circle image plate, reducing the intensity variation due to preferred orientation, but with a loss of time resolution (1−2 min/plate). The wavelength, sample-to-detector distance, tilting angle of the IP and zero shift position of the IP for the data collection were calibrated to the LaB_6 standard using the 'fit2d' software package to analyze the full Debeye-Scherrer rings of the MAR data.[43] The time-resolved data collected on the TIP system were processed using software written by Poul Norby for X7B.[42] Powdered samples placed in 0.7 mm fused silica capillaries were affixed to a gas line with Swage Lock fittings and aligned on a goniometer head.[44] The ethylene pressure was metered with an electronically controlled gas manifold. Temperature control was achieved with an Oxford cryostream. The experiments of Figures 4−5 and Supporting Figure 2 were obtained using the TIP detector and the experiment of Figure 3 was collected using the MAR detector.

Single-Crystal X-ray Diffraction of $(C_2H_4)_2CuAlCl_4$. A single crystal of **et-2** was obtained from a reaction in which approximately 250 mg of α−$CuAlCl_4$ was exposed to 1500 Torr of ethylene for 6 h, then the thick walled fused silica reaction tube was frozen in liquid N_2 and flame sealed such that an ethylene pressure of approximately 3000 Torr was obtained at ambient temperature. The reaction was heated to 75 °C to melt the sample and then cooled to room temperature. The sample was periodically examined over a period of five months when pale yellow crystals were observed to form. The crystals were immediately covered with ethylene saturated Apiezon grease when the reaction tube was opened. A single crystal (0.20 × 0.18 × 0.12 mm) was quickly mounted on the end of a glass fiber and transferred to the diffractometer and cooled to −135 °C in a nitrogen cold stream. Diffraction data were measured using an Enraf-Nonius CAD4-MACH diffractometer. The unit cell dimensions were determined by a fit of 25 well-centered reflections and their Friedel pairs with $33° < 2(\theta) < 36°$. A quadrant of unique data and their Bijvoet pairs were collected using the omega scan mode in a nonbisecting geometry. Three standard reflections were measured every 4800 s of X-ray exposure time, and the data were scaled using a 5 point smoothing routine fit to the intensity check reflections. The intensity data was corrected for Lorentz and polarization effects. Additional unit cell parameters and reflections for 24 Friedel pairs were measured at −101, −88, −79, −66, −55, −44, and −33 °C to search for a monoclinic/orthorhombic phase transition. No transformation was observed prior to the softening of the Apiezon grease at −10 °C.

Systematic absences were found to be consistent with the space groups $P2_1/c$ and *Pc*. The data were reduced using routines from the NRCVAX set of programs. All non-hydrogen atoms were located in the *Pc* space group by direct methods using the SIR92 program.[45] The structure was refined using the NRCVAX suite of programs.[46] Five of the eight hydrogen atoms bound to the ethylenes were found from the difference Fourier map and the three remaining hydrogens on two carbons were added in calculated positions. The C−H distances were fixed at 0.96 Å and the bond angles allowed to refine freely. A full matrix least squares refinement based on *F* used 2926 unique reflections ($I > 1.0\,\sigma(I)$) and gave a final refinement with *R* factors of $R = 0.030$ and $R_w = 0.034$. The absolute structure was refined to a Flack parameter of 0.33(1). The absolute structure was confirmed by a Bijvoet analysis of 200 total measurements, of which the (Fo+ − Fo−) for 196 cases have the same sign as (Fc+ − Fc−), and the opposite sign in only four cases.

Single-Crystal X-ray Diffraction of β-$(C_2H_4)CuAlCl_4$. A single of crystal of **β-et-1** was grown in situ for a structural solution. A 1 mm capillary was hand drawn off the end of a fused silica tube with a valve for attachment to a gas line. A plug of glass wool separated the capillary from the primary tube volume. The reaction tube was charged with about 0.5 g α-$CuAlCl_4$ and 1000 Torr of ethylene. Using a combination of heating with a hot air gun and cooling the tip of the capillary with liquid N_2, the viscous yellow liquid was drawn into the capillary. The capillary was frozen in liquid N_2 then flame sealed. The sealed sample was repeatedly melted and allowed to cool over a period of months in an effort to grow single crystals. Along with multiple smaller crystallites a light yellow ethylene/$CuAlCl_4$ adduct single crystal (0.8 × 0.8 × 0.8 mm) was grown. Diffraction data for this in situ grown crystal were collected on the X7b NSLS beamline, using the *MAR*345 image plate detector, using the full 345 mm diameter (150 micron pixels), at 100 K with wavelength of 0.94 Å. A total of 67 images were measured. A unit cell was determined separately for each recorded image. The cell constants (on the basis of all 67 images) are mean values and the esds come from repeated analysis of the determinations.

Systematic absences were consistent with the space group $Pna2_1$, which was subsequently confirmed in the structural refinement. The structure was solved and refined using the SHELX suit of programs.[47] All non-hydrogen atoms were found by direct methods and difference Fouriers, and hydrogen atoms were placed in calculated positions. Refinement was performed on F^2 for all reflections, except for those flagged by the user for potential systematic errors, and gave a final refinement with *R* factors of $R = 0.037$ and $wR = 0.142$. The absolute structure was refined to a Flack parameter of 0.01(1).

Multinuclear MAS NMR. ^1H, ^{13}C, ^{27}Al, and ^{63}Cu MAS NMR experiments were performed using a double-tuned Chemagnetics 5 mm probe in a CMX-360 spectrometer at operating frequencies of 360, 90.5, 93.8, and 95.5 MHz, respectively. The radio frequency field strengths were approximately 60 kHz. ^1H, ^{13}C MAS spectra were acquired with 90° single-pulse sequences, and ^{27}Al and ^{63}Cu spectra with small flip angles (pulse width of 1 μs). Spinning rates of 10.0 kHz and recycle delays of 2, 20, 1, and 1 s were used for acquisition of ^1H, ^{13}C, ^{27}Al and ^{63}Cu spectra, respectively, unless specifically noted. The chemical shifts are referenced relative to chloroform (7.2 ppm for ^{13}C), TMS (0 ppm for ^1H), a saturated aqueous $Al_2(SO_4)_3$ solution (0 ppm for ^{27}Al), and solid CuCl (−319 ppm for ^{63}Cu) as external standards. $^1H \rightarrow {}^{13}C$ CP MAS NMR spectra were collected with radio frequency fields matched at 40 kHz, contact time of 0.5 ms, pulse delay of 2 s, and spinning speed of 3.0 kHz. $^{13}C/^{65}Cu$ TRAPDOR NMR was carried out on a triple-tuned Chemagnetics 5 mm probe in the same CMX-360 spectrometer with ^{65}Cu resonating at 102.1 MHz. A pulse sequence taking advantage of $^1H \rightarrow {}^{13}C$ cross polarization was used in the TRAPDOR experiment.[34] A $^{13}C/^{65}Cu$ TRAPDOR experiment, and not a $^{13}C/^{63}Cu$ TRAPDOR NMR experiment was performed, due to the larger separation, and hence isolation, of the ^{13}C and ^{65}Cu channels. Other acquisition conditions were the same as those for $^1H \rightarrow {}^{13}C$ CP MAS NMR.

The simulation of the second-order quadrupolar line shape of ^{27}Al central transition was performed with the WSolids NMR simulation package written by K. Eichele of Dalhousie University, Canada.

(42) Norby, P. *J. Appl. Crystallogr.* **1997**, *30*, 21−30.
(43) (a) Hammersley, A. P. *FIT2D: An Introduction and Overview*; ESRF Internal Report, ESRF97HA02T; European Synchrotron Radiation Facility: Grenoble Cedex, France, 1997. (b) Hammersley, A. P. *FIT2D V9.129 Reference Manual V3.1*; ESRF Internal Report, ESRF98HA01T; European Synchrotron Radiation Facility: Grenoble Cedex, France, 1998.
(44) Norby, P. In-situ Time-Resolved Synchrotron Powder Diffraction Studies of Syntheses and Chemical Reactions. In *European Powder Diffraction*; Cernik, R. J., Delhez, R., Mittemeijer, E. J., Eds.; Materials Science Forum Vol. 228 until 231: Trans Tech Publications: Zürich, Switzerland, 1996; pp 147−152.
(45) Altomare, A.; Burla, M. C.; Camulli, G.; Cascarano, G.; Giacovazzo, C.; Guagliardi, A.; Polidori, G. *J. Appl. Crystallogr.* **1994**, *27*, 435.
(46) Gabe, E. J.; Le Page, Y.; Charland, J.-P.; Lee, F. L.; White, P. S. *J. Appl. Crystallogr.* **1989**, *22*, 384.
(47) Sheldrick, G. M. SHELX, a Program for Crystal Structure Refinement, University of Göttingen, Germany.

Diffuse Reflectence Spectroscopy. Diffuse reflectance measurements were carried out on a Cary 3e UV−vis spectrophotometer equipped with an integrating sphere. Spectra were measured with respect to a pressed poly(tetrafluoroethylene) powder standard. Reflectance intensities were collected as the remission function, $F(R_\infty) = (1 - R_\infty)^2/2R_\infty$ (based on the Kubelka−Munk theory of diffuse reflectance)[48] versus wavenumber. For measurement of the reflectance upon gas sorption/desorption, samples were prepared by grinding 0.06 g of α-$CuAlCl_4$ with 2 g of ground fused silica particles (300−800 μm) together. Powdered samples were then placed in a 1 × 10 mm cuvette which was connected to a gas/vacuum manifold.

Acknowledgment. Dr. Paul Boyle is acknowledged for collection of the single crystal data for **et-2**; Mr. Anthony Wong, a high-school student in the Howard Hughes RISE program assisted with the diffuse reflectance measurements. D. O. was sponsored through the ACS project SEED program. Support for this work via the contracts NSF DMR-0072828, and DOE-BES DEAC0298CH10086, and DEFG0296ER14681 is gratefully acknowledged. The NSLS is supported by the division of materials sciences of DOE. J.D.M. and C. P. G. are Cottrell Scholars of the Research Corporation

Supporting Information Available: X-ray crystallographic data for ***β*-et-1** and **et-2** are available in .cif format. Six figures are given describing the adsorption isotherms for $CuGaCl_4$, the low-temperature TRXRD sorption of ethylene by $CuAlCl_4$, the proposed structural model for **α-et-1**, the powder X-ray diffraction, the ^{63}Cu MAS NMR of **α-et-1** and the structural relationship between α-$CuAlCl_4$ and **α-et-1**. This material is available free of charge via the Internet at http://pubs.acs.org.

JA036172O

(48) Wendlandt, W. W.; Hecht, H. G. *Reflectance Spectroscopy*; Interscience: New York, 1966; Chapter 3.